Cell Reports

Article

Extracellular Granzyme A Promotes Colorectal Cancer Development by Enhancing Gut Inflammation

Graphical Abstract

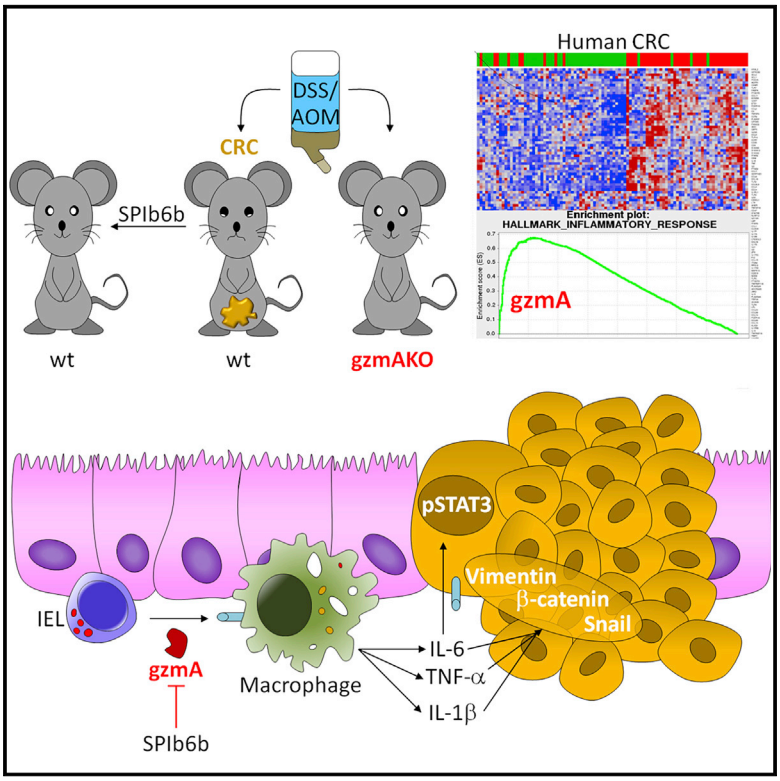

Highlights

- *GZMA* mRNA expression correlates with inflammation in human CRC patients
- GzmA deficiency reduces gut inflammation and colorectal cancer development
- Therapeutic GzmA inhibition in WT mice reduces colorectal cancer development
- GzmA induces IL-6 production in macrophages activating pSTAT3 in colon cancer cells

Authors

Llipsy Santiago, Marta Castro, Rebeca Sanz-Pamplona, ..., Sunil Metkar, Maykel A. Arias, Julian Pardo

Correspondence

maykelariascabrero@gmail.com (M.A.A.), pardojim@unizar.es (J.P.)

In Brief

Santiago et al. show that extracellular granzyme A (GzmA) contributes to gut inflammation and colorectal cancer (CRC) development by promoting IL-6 production in macrophages. Therapeutic inhibition of GzmA attenuates inflammation and CRC development, suggesting that GzmA could be useful to treat gut inflammation and prevent CRC.

Santiago et al., 2020, Cell Reports *32*, 107847
July 7, 2020
https://doi.org/10.1016/j.celrep.2020.107847

CellPress

Cell Reports

CellPress
OPEN ACCESS

Article

Extracellular Granzyme A Promotes Colorectal Cancer Development by Enhancing Gut Inflammation

Llipsy Santiago,[1] Marta Castro,[2] Rebeca Sanz-Pamplona,[3] Marcela Garzón,[1] Ariel Ramirez-Labrada,[1] Elena Tapia,[17] Víctor Moreno,[3,16] Elena Layunta,[4] Gabriel Gil-Gómez,[5] Marta Garrido,[5] Raúl Peña,[5] Pilar M. Lanuza,[1] Laura Comas,[6] Paula Jaime-Sanchez,[1] Iratxe Uranga-Murillo,[1] Rosa del Campo,[7] Pablo Pelegrín,[15] Eric Camerer,[19] Luis Martínez-Lostao,[1,8,13,14] Guillermo Muñoz,[8] José A. Uranga,[9] Anabel Alcalde,[4,21] Eva M. Galvez,[6] Angel Ferrandez,[11] Phillip I. Bird,[18] Sunil Metkar,[10] Maykel A. Arias,[6,22,*] and Julian Pardo[1,12,13,14,20,23,*]

[1]Fundación Instituto de Investigación Sanitaria Aragón (IIS Aragón), Biomedical Research Centre of Aragon (CIBA), 50009 Zaragoza, Spain
[2]Department of Pharmacology and Physiology, Faculty of Health and Sports Sciences, University of Zaragoza, 22002 Huesca, Spain
[3]Unit of Biomarkers and Susceptibility, Oncology Data Analytics Program (ODAP), Catalan Institute of Oncology (ICO), Oncobell Program, Bellvitge Biomedical Research Institute (IDIBELL) and CIBERESP, L'Hospitalet de Llobregat, Barcelona, Spain
[4]Department of Pharmacology and Physiology, Faculty of Veterinary, University of Zaragoza, 50013 Zaragoza, Spain
[5]Institut Hospital del Mar d'Investigacions Mèdiques (IMIM), 08003 Barcelona
[6]Instituto de Carboquímica ICB-CSIC, 50018 Zaragoza, Spain
[7]Department of Microbiology, University Hospital Ramón y Cajal & Instituto Ramón y Cajal de Investigación Sanitaria (IRYCIS), 28034 Madrid, Spain
[8]Department of Immunology, University Clinic Hospital Lozano Blesa, 50009, Zaragoza, Spain and Department of Pathology, University Clinic Hospital Lozano Blesa, University of Zaragoza, IIS Aragón, CIBEREHD, 50009 Zaragoza, Spain
[9]Department of Basis Health Sciences, Faculty of Health Sciences, Rey Juan Carlos University, 28922 Madrid, Spain
[10]XEME Biopharma Inc., Lombard, IL, USA
[11]Service of Digestive Diseases, University Clinic Hospital Lozano Blesa, University of Zaragoza, IIS Aragón, CIBEREHD, Zaragoza, Spain
[12]Aragon I+D Foundation (ARAID), Zaragoza, Spain
[13]Nanoscience Institute of Aragon (INA), University of Zaragoza, 50018 Zaragoza, Spain
[14]Department Biochemistry and Molecular and Cell Biology and Department Microbiology, Preventive Medicine and Public Health, University of Zaragoza, 50009 Zaragoza, Spain
[15]Unidad de Inflamación Molecular y Cirugía Experimental, Instituto Murciano de Investigación Biosanitaria IMIB-Arrixaca, Hospital Clínico Universitario Virgen de la Arrixaca, Murcia, Spain
[16]Department of Clinical Sciences, Faculty of Medicine and Health Sciences, University of Barcelona, Barcelona, Spain
[17]Animal Unit, University of Zaragoza, 50009 Zaragoza, Spain
[18]Department of Biochemistry and Molecular Biology, Biomedicine Discovery Institute, Monash University 3800 Melbourne, Australia
[19]Université de Paris, Paris Cardiovascular Research Center, INSERM U970, 75015 Paris, France
[20]CIBER-BBN, Madrid, Spain
[21]Deceased September 2015
[22]Present address: Instituto de Carboquímica ICB-CSIC, 50018 Zaragoza, Spain
[23]Lead Contact
*Correspondence: maykelariascabrero@gmail.com (M.A.A.), pardojim@unizar.es (J.P.)
https://doi.org/10.1016/j.celrep.2020.107847

SUMMARY

If not properly regulated, the inflammatory immune response can promote carcinogenesis, as evident in colorectal cancer (CRC). Aiming to gain mechanistic insight into the link between inflammation and CRC, we perform transcriptomics analysis of human CRC, identifying a strong correlation between expression of the serine protease granzyme A (GzmA) and inflammation. In a dextran sodium sulfate and azoxymethane (DSS/AOM) mouse model, deficiency and pharmacological inhibition of extracellular GzmA both attenuate gut inflammation and prevent CRC development, including the initial steps of cell transformation and epithelial-to-mesenchymal transition. Mechanistically, extracellular GzmA induces NF-κB-dependent IL-6 production in macrophages, which in turn promotes STAT3 activation in cultured CRC cells. Accordingly, colon tissues from DSS/AOM-treated, GzmA-deficient animals present reduced levels of pSTAT3. By identifying GzmA as a proinflammatory protease that promotes CRC development, these findings provide information on mechanisms that link immune cell infiltration to cancer progression and present GzmA as a therapeutic target for CRC.

INTRODUCTION

Colorectal cancer (CRC) is the second-leading cause of cancer cell death in developed countries and the third-most common cancer. If not detected early and surgically removed, pharmacological treatment has low efficacy and resistance/recurrence often occurs. A better understanding of the mechanisms involved in CRC development may identify novel targets and improve the current therapies against this lethal cancer.

Chronic inflammation represents an adverse prognostic factor for the progression of solid tumors like CRC. It is well known that patients suffering from ulcerative colitis (UC) have a higher risk of CRC (Bernstein et al., 2001; Eaden et al., 2001). Inflammation is also involved in sporadic and hereditary CRC (Crusz and Balkwill, 2015; Fearon and Vogelstein, 1990; Mantovani, 2018; Shalapour and Karin, 2015). The connection between inflammation and tumorigenesis is mediated by cells of the innate and adaptive immune system, including macrophages, eosinophils, innate lymphoid cells (ILCs), and specific subsets of $CD4^+$ T cells (Kirchberger et al., 2013; Lasry et al., 2016; Powell et al., 2017; Shalapour and Karin, 2015). Tumorigenesis is also influenced by the composition of the gut microbiota (Brennan and Garrett, 2016; Powell et al., 2017). Reactive oxygen species (ROS); lipid mediators produced by cyclooxygenase activity, such as prostaglandin E2 (PGE_2); and several proinflammatory cytokines are involved in CRC development (Lasry et al., 2016; Shalapour and Karin, 2015). All these molecules contribute to epithelial cell transformation and tumor progression through the activation of genetic and signaling pathways, including nuclear factor κB (NF-κB), pSTAT3 (phospho-Signal transducer and activator of transcription 3), Wnt, β-catenin, or K-ras (Kaler et al., 2009; Karin, 1998; Li and Laterra, 2012; Shalapour and Karin, 2015; Shenoy et al., 2012; Yu et al., 2009). However, little is known about the molecular mechanism or mechanisms by which the immune system orchestrates the production of these proinflammatory factors during gut inflammation and CRC. Thus, pharmacological regulation of inflammation to prevent and/or improve CRC treatment is nonspecific and associated with serious side effects related to infection and (paradoxically) tumor progression (Yang et al., 2017).

Granzymes (Gzms) are a family of serine proteases (5 in human and 11 in mice) mainly expressed by cytotoxic cells (natural killer [NK] cells and cytolytic $CD8^+$ T cells). Some members of this family are present in other immune cells, like $CD4^+$ T cells, macrophages, basophils, or mast cells, and non-immune cells, like chondrocytes, keratinocytes, and pneumocytes (Afonina et al., 2010; Arias et al., 2017; Martínez-Lostao et al., 2015; Turner et al., 2019; Voskoboinik et al., 2015). Some Gzms exert their biological effects by inducing death of tumor or virus-infected cells (Chowdhury and Lieberman, 2008) after being delivered intracellularly by the pore-forming protein perforin (Bovenschen and Kummer, 2010; Pardo et al., 2009). However, during the past few years, it has become clear that human and mouse Gzms, namely, GzmA, GzmM, or GzmK, are involved in processes unrelated to cytotoxicity—for example, in the regulation of the inflammatory response (Afonina et al., 2010; Anthony et al., 2010b; Martínez-Lostao et al., 2015;Turner et al., 2019 Wensink et al., 2015) or in processes related to their ability to degrade extracellular matrix proteins when released in the extracellular milieu, as reported for GzmB (Arias et al., 2017; Granville, 2010; Turner et al., 2019).

The relationship of Gzms with colon carcinogenesis is unclear. GzmB provides cytotoxic activity against cancer cells and is a positive prognostic marker in human CRC (Galon et al., 2012; Pagès et al., 2005; Salama et al., 2011). By contrast, the biological role of the other major Gzm, GzmA, during CRC is unknown.

In this study, in searching for molecules involved in inflammation during CRC, we performed transcriptomics analysis of tissue samples from CRC patients and found a strong correlation between *GZMA* expression and inflammatory genes in most molecular subtypes (consensus molecular subtypes [CMSs]). To assess the relevance of this finding, we used the well-characterized dextran sodium sulfate and azoxymethane (DSS/AOM) mouse model to demonstrate that both GzmA deficiency and therapeutic GzmA inhibition attenuate gut inflammation and protect mice from CRC development. Inflammation and gut permeability in steady-state conditions were unaffected by GzmA deficiency, confirming that reduction of inflammatory response and CRC is not related to intestinal phenotypic changes in the absence of GzmA. Instead, it correlated with the ability of extracellular GzmA to induce macrophage interleukin (IL) 6 production.

These results show that GzmA, acting in the extracellular environment, regulates the inflammatory response in the gut and is a key mediator in the development of inflammatory CRC, thus identifying a new molecular mechanism involved in inflammation-induced CRC and validating it as a potential new therapeutic target. Considering that GzmA-deficient mice can control experimental infections (Arias et al., 2017), our findings indicate that targeted GzmA inhibition might be useful to prevent and treat CRC in a more selective way than current immunosuppressive anti-inflammatory treatments.

RESULTS

A Positive Correlation between *GZMA*, but Not *GZMB*, and Inflammation in Human CRC Samples

An analysis of mRNA expression was performed in 98 CRC tumor samples from stage 2 patients undergoing surgery (hereafter Colonomics) (Sanz-Pamplona et al., 2014). The transcriptomics data were used to determine whether *GZM* expression correlated with pathways involved in CRC, focusing on the two major GZMs, *GZMA* and *GZMB*. As shown in the gene set enrichment analysis (GSEA), *GZMA* was clearly co-expressed with genes related to inflammatory pathways such as interferon gamma (IFN-γ) and interferon alpha response, IL-2, and tumor necrosis factor alpha (TNF-α) signaling or inflammatory response. An enrichment of genes involved in the epithelial-to-mesenchymal transition (EMT) pathway was also detected (Figure S1B; Table S2).

Based on these encouraging results, an inflammation score was calculated for each sample in the Colonomics dataset (Figure 1A) and in an extended dataset comprising 566 human CRC samples (hereafter GEO: GSE39582; Figure 1B). A highly

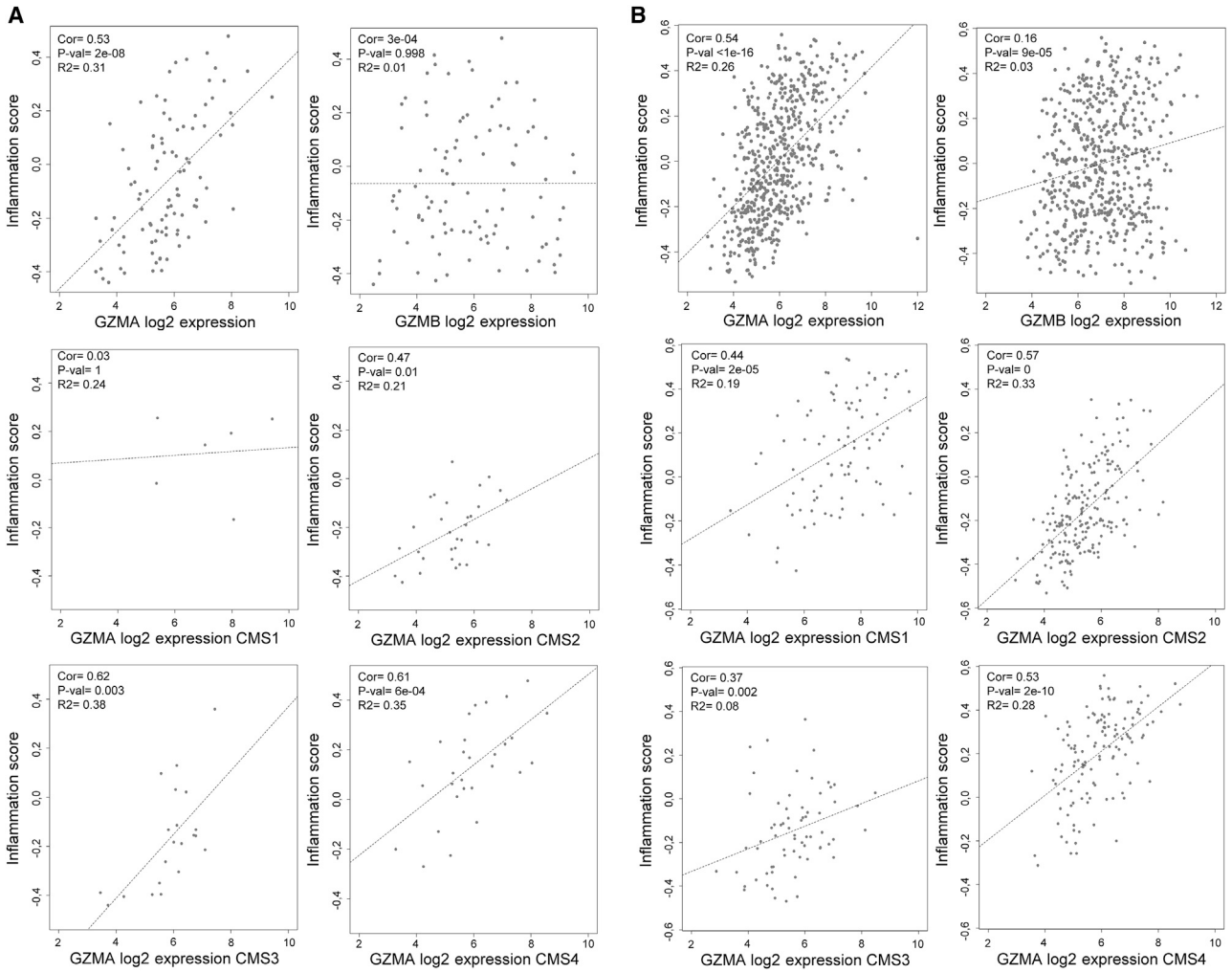

Figure 1. *GZMA* Expression Positively Correlates with Inflammation Score in Human Samples Regardless of Their Molecular Subtype

(A and B) Levels of *GZMA* mRNA are highly correlated with inflammation score in both Colonomics (A) and GEO: GSE39582 (B) datasets. In contrast, levels of *GZMB* mRNA are not correlated with the inflammation score (A and B, upper panels). The x axes indicate the intensity of *GZM* mRNA expression. Middle and lower panels show correlation between *GZMA* expression level (x axis) and inflammation score stratified by CMS subgroup in Colonomics (A) and GEO: GSE39582 (B) datasets. The x axes indicate *GZMA* mRNA expression classified according CMS groups as indicated. In all plots, Spearman's rho correlation value, correlation p value, and R-squared coefficients are depicted. Linear regression lines are in dashed gray.

significant positive correlation between inflammation score and *GZMA* expression existed in both datasets. By contrast, no correlation was observed between inflammatory score and *GZMB* expression.

To evaluate whether correlation between *GZMA* expression and inflammation was restricted to a specific CMS, the analyses were repeated and the samples were stratified by CMS status in both datasets (Figures 1A and 1B, middle and lower panels). Significant correlation was observed in all CMS groups in both datasets, with the exception of CMS1 in Colonomics, probably because of the low number of samples. This result confirms that the presence of *GZMA* correlates with the inflammatory status in all molecular subtypes of colon cancer. *GZMA* gene expression did not correlate with prognosis (time until tumor recurrence) in the Colonomics cohort (data not shown). However, the Colonomics cohort only includes stage 2 patients, who mostly recover after surgery.

GzmA Is Elevated in Colon Tissue during CRC Progression in Mice

To address the relevance of the findings in human samples and to determine whether the protease plays a causal role in CRC progression, we addressed whether attenuation of GzmA would affect CRC development in mice. Combined administration of DSS/AOM is a well-characterized protocol of inducing inflammatory CRC in mice that mimics CRC development in humans. With the exception of metastatic transformation, it reproduces all stages and molecular features (mutations and EMT) of human colorectal (CR) carcinogenesis, including aberrant crypt foci, microadenoma, adenoma, and carcinoma (De Robertis et al., 2011; Fichtner-Feigl et al., 2015; Takahashi et al., 1998; Yu et al., 2009).

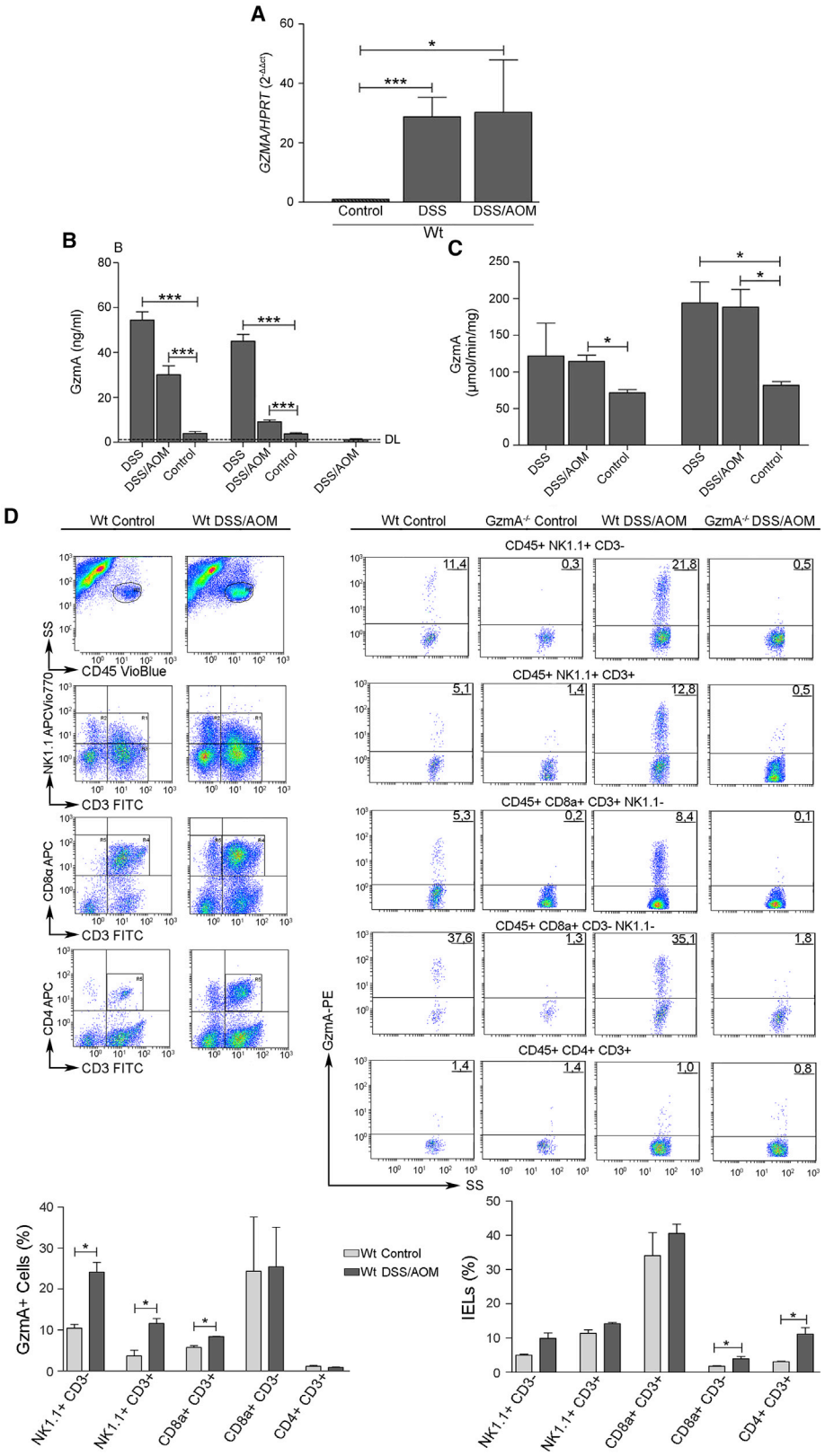

(legend on next page)

As shown in Figure 2A, *GZMA* mRNA expression was significantly elevated in mice developing both CRC (DSS/AOM) and chronic gut inflammation (DSS), which correlated with significantly increased protein level in distal and proximal colonic explant cultures from DSS/AOM- and DSS-treated wild-type (WT) mice (Figure 2B). Notably, GzmA was presented in supernatants in active form, with higher enzymatic activity in samples from treated animals than in those from untreated WT control mice (Figure 2C). As expected, GzmA was not detected in supernatants from GzmA knockout ($GzmA^{KO}$) animals.

As shown in Figure 2D, the abundance of intraepithelial NK/ILC1 cells (CD45+/NK1.1+/CD3−), NKT (natural killer T) cells (CD45+/NK1.1+/CD3+), and CD8+ T cells (CD45+/CD8α+/CD3+) expressing GzmA was significantly increased in DSS/AOM-treated animals. The proportion of CD8α+/CD3− cells expressing GzmA did not increase during treatment with DSS/AOM. This population could represent resident CD8αα+/TCR−/CD3− intraepithelial lymphocytes (IELs) (Olivares-Villagómez and Van Kaer, 2018). CD4+T lymphocytes (CD45+/CD4+/CD3+), which did not express GzmA, increased significantly in DSS/AOM-treated animals (Figure 2D). GzmA expression was not detected in cells from $GzmA^{KO}$ animals, confirming specificity of detection.

CRC Development Is Reduced in GzmA-Deficient Mice

Next, we monitored CRC development in WT and $GzmA^{KO}$ animals macroscopically and microscopically. As shown in Figure 3A, tumor incidence was significantly higher in WT mice than in $GzmA^{KO}$ mice. Furthermore, in $GzmA^{KO}$ mice that developed macroscopic tumors, tumor number and size were both significantly lower than in WT mice. The reduction of CRC development in $GzmA^{KO}$ mice was similar to that observed in WT mice treated with the TNF-α-blocking agent Enbrel (Figure S2A), which has been previously shown to inhibit CRC development in this model (Popivanova et al., 2008). When the experiments were repeated using littermate controls, a similar result was found. $GzmA^{KO}$ mice developed fewer tumors and presented fewer clinical symptoms and less intestinal damage than littermate controls (Figure S3). Therefore, to reduce the number of animals employed, inbred WT B6 animals were used as controls for the next experiments.

As shown in Figure 3B, at the end of the experiment (56 days), all DSS/AOM-treated WT mice presented epithelial cell transformation, although at different stages (Figure S4A). Adenocarcinoma was present in 50%, and dysplasia of low and high degree was present in 30% and 20%, respectively. By contrast, 20% of $GzmA^{KO}$ mice showed no CRC or dysplasia and only 20% progressed to adenocarcinoma. Similar differences were observed at early time points after initiating DSS/AOM treatment. At day 47, 40% of $GzmA^{KO}$ mice did not present any type of tumor and the rest only presented dysplasia. In contrast, all WT mice presented dysplasia and 13% presented carcinoma. At day 28, dysplasia was observed in only 37% of $GzmA^{KO}$ mice, but it was already evident in 60% of WT mice. These results confirm that GzmA plays a critical role in development of CRC and likely in the perpetuation of the cancerous state.

Similar results were obtained when we analyzed proliferation (Ki-67) and EMT (vimentin, β-catenin, and SNAIL-1) markers by immunohistochemistry, confirming the critical role of GzmA in epithelial cell transformation and CRC development (Figures 3C and 3D; Figure S4B). Analyses were performed at day 28 (4 weeks) of DSS/AOM treatment, after which EMT begins (De Robertis et al., 2011; Takahashi et al., 1998). Vimentin was expressed in a large number of cells, especially in the areas of dysplasia of WT animals treated with DSS/AOM. The absence of GzmA significantly reduced the number of vimentin-positive cells in the mucosa and submucosa layers. Similarly, DSS/AOM-exposed animals showed a significant increase in cytoplasmic and nuclear β-catenin in epithelial cells, whereas $GzmA^{KO}$ animals showed β-catenin staining restricted mostly to the cell membrane. SNAIL-1 expression was also increased in DSS/AOM-treated mice, showing high positivity in the lamina propria and the connective tissue. In $GzmA^{KO}$ mice, the staining pattern was similar to that in untreated control mice (Figure S4B), with few positive cells in the connective tissue.

Finally, an increase in the number of proliferative cells could be seen with the Ki-67 marker. In DSS/AOM-treated WT animals, the positivity was not restricted to the basal area of the colonic glands, but it reached the vicinity of the apical zone in certain cases. In contrast, DSS/AOM-treated $GzmA^{KO}$ animals showed this marker restricted to the basal area, similar to the untreated control animals (Figure S4B). The expression of all markers in untreated $GzmA^{KO}$ and WT control animals was similar (Figure S4B). The differences between WT and $GzmA^{KO}$ animals were statistically significant in all cases (Figure 3D). Strong Ki-67, vimentin, and

Figure 2. Levels of GZMA mRNA and Active Protein Are Increased in Explants from DSS- and DSS/AOM-Treated Mice, with Expression of GzmA by IELs

Male C57BL/6 WT mice were treated with DSS and DSS/AOM, as described in Method Details, and sacrificed at day 56.

(A) mRNA levels of *GZMA* were determined by qRT-PCR (normalized to the amount of *HPRT* mRNA). The relative gene expression levels were expressed as the fold difference ($2^{-\Delta\Delta Ct}$), as described in Method Details. Data are presented as mean ± SEM from 3 biological replicates. Statistical analyses were performed by one-way ANOVA test with Bonferroni's post-test. *$p < 0.05$; ***$p < 0.001$.

(B) Colonic tissue samples (30 mg) were cultured during 24 h, supernatant was collected, and GzmA was quantified by ELISA in proximal and distal colon.

(C) GzmA enzymatic activity was determined. Specific activity was calculated by subtracting the residual unspecific tryptase-like activity detected in $GzmA^{KO}$ animals used as control from the activity observed in WT mice. Data are presented as mean ± SEM from 5 biological replicates performed in 3 independent experiments. Statistical analyses were performed by one-way ANOVA test with Bonferroni's post-test. *$p < 0.05$; ***$p < 0.001$.

(D) IELs were isolated from WT and $GzmA^{KO}$ mice at day 49 of treatment with DSS/AOM, as indicated in Method Details, and stained with a combination of anti-CD3-FITC, anti-CD8a-APC, anti-NK1.1-APC-Vio770, and anti-CD45-VioBlue antibodies. Intracellular GzmA expression was analyzed using anti-GzmA-PE antibody. A representative experiment is shown. Numbers in dot plots represent the percentage of GzmA-positive cells for each IEL phenotype. IELs from untreated WT and $GzmA^{KO}$ mice were isolated as control. Data in bar graphs represent the mean ± SEM of GzmA-positive cells of each IEL phenotype (left) and the percentage of each subtype of IELs isolated from treated and untreated WT mice (right) from two independent experiments. Statistical analyses were performed by Student's t test, comparing treated WT mice with untreated WT mice. *$p < 0.05$.

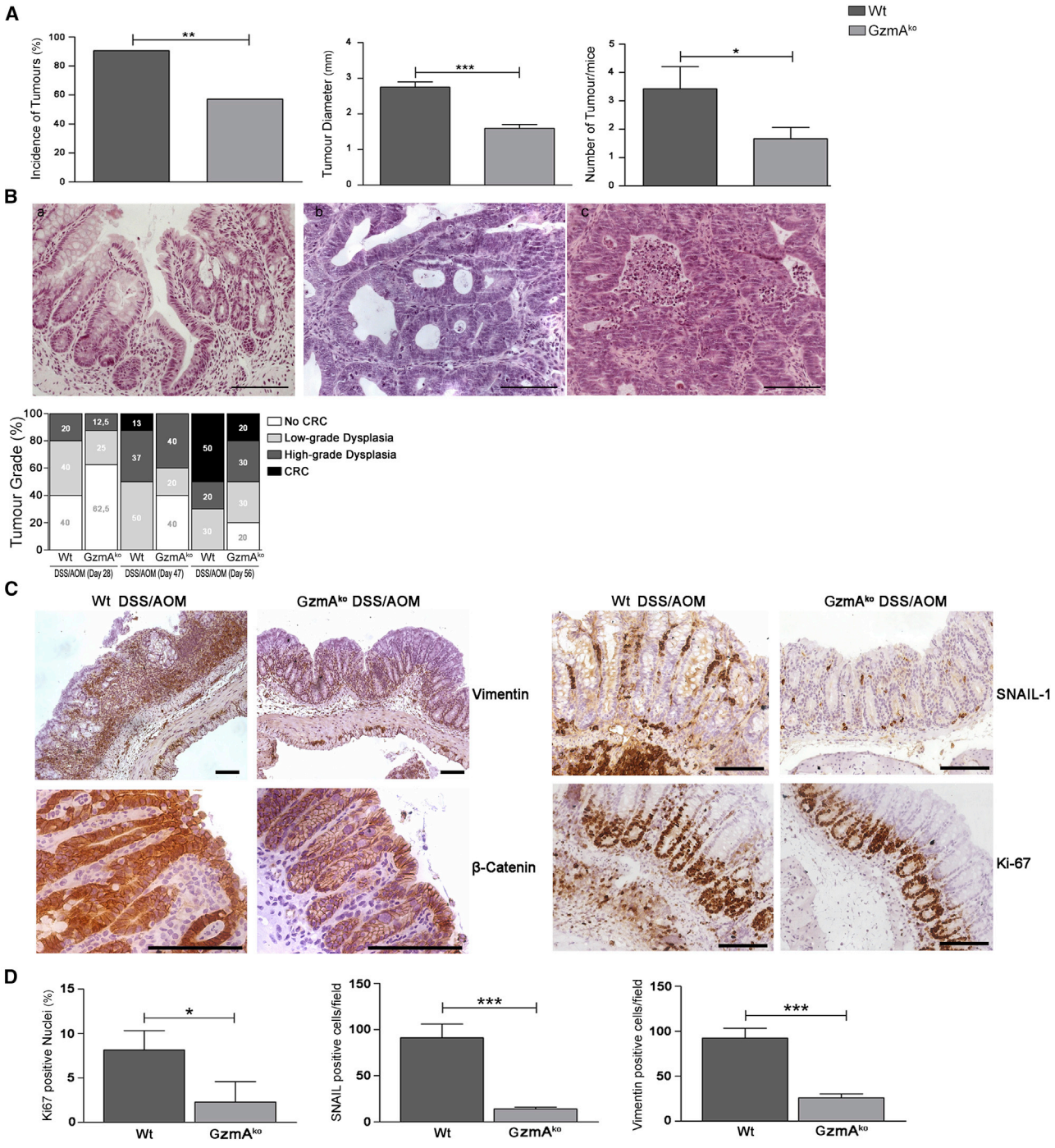

Figure 3. CR Carcinoma Development in DSS/AOM-Treated Mice

CRC was induced in male C57BL/6 WT and GzmA^{KO} mice with DSS and AOM, as described in STAR Methods.

(A) Number of animals bearing tumors (tumor incidence), tumor diameter, and number of tumors per animal were evaluated. Data are presented as mean ± SEM of 31 (WT) and 24 (GzmA^{KO}) biological replicates (individual mice) in 4 independent experiments. Statistical analyses were performed by one-way ANOVA test with Bonferroni's post-test. *$p < 0.05$; **$p < 0.01$; ***$p < 0.001$.

(B) Colonic tissues were removed and processed for histopathology. Representative microphotographs of H&E-stained colonic sections show low-grade dysplasia (a), high-grade dysplasia (b), and carcinoma (c). Scale bars, 100 μm. Histologic tumor grade was established in WT and GzmA^{KO} mice and represented as the percentage of mice with the indicated tumor grade (highest tumor grade found) within each group.

(legend continued on next page)

SNAIL-1 positivity was observed in connective-tissue-associated fibroblast-like cells only in DSS/AOM-treated WT mice, which is in line with the changes observed in connective tissue before EMT occurs (Kalluri and Weinberg, 2009).

Inflammation Is Reduced in Colon Tissue from GzmA-Deficient Mice during CRC Development

It is well known that during DSS/AOM-induced CRC, tumors almost exclusively appear in the distal part of the colon. Thus, to test the effect of GzmA deficiency on intestinal inflammation independent of tumor development, the production of proinflammatory cytokines was analyzed in both proximal and distal colonic tissue. This is important, because once tumors develop, the inflammatory reaction is downregulated in tumoral tissue, which might mask the potential contribution of GzmA to intestinal inflammation and CRC. Indeed, as shown in Figure 4A, levels of proinflammatory cytokines (IL-1β, TNF-α, IFN-γ, IL-6, and IL-17) were higher in proximal colon compared with distal colon. In proximal colon, all proinflammatory cytokines tested were significantly higher in WT animals than in GzmA^{KO} mice. In distal colon, proinflammatory cytokines were also significantly higher in DSS/AOM-treated WT mice than in untreated WT B6 mice, although in this case differences between WT and GzmA^{KO} animals were only significant for TNF-α, IFN-γ, and IL-6. However, IL-10, an anti-inflammatory cytokine involved in maintaining intestinal homeostasis (Glocker et al., 2011; Kühn et al., 1993), was significantly lower in WT mice than in GzmA^{KO} mice in both proximal and distal colon. In contrast to WT mice, only IL-17 was significantly increased in DSS/AOM-treated GzmA^{KO} animals relative to untreated controls.

As shown in Figure 4B, *COX-2* mRNA expression and PGE_2 production were significantly higher in WT mice compared with untreated controls and compared with GzmA^{KO} mice, confirming that COX-2 activity was reduced in the absence of GzmA.

The contribution of inflammatory cytokines and PGE_2 to CR carcinogenesis is critically modulated by the transcription factor STAT3, which is activated upon phosphorylation. As shown in Figure 4C, pSTAT3 was induced in cells of the mucosa and submucosa of DSS/AOM-treated animals, with many positive cells in the areas of dysplasia. A significant decrease in positivity was observed in the GzmA^{KO} group treated with DSS/AOM, in comparison with WT mice, although the number of pSTAT3-positive cells remained higher than in untreated animals (Figure S4B). Thus, protection against CRC development granted by GzmA deficiency consistently correlates with reduction in the carcinogenic proinflammatory state in gut.

Analyses of gut microbiota in both WT and GzmA^{KO} mice, employing 16S rDNA sequencing, revealed that both mouse strains present an almost identical composition of bacterial gut microbiota at the genus level (Figure S5), thus ruling out differences in the composition of the gut microbiome as a factor modulating the increased resistance of GzmA^{KO} mice to inflammatory CRC development. This finding is not unexpected, because independent recent studies indicate that mice hosted at the same animal facility contain identical microbiota due to the same feed and environmental stress conditions (Ericsson et al., 2018; Montonye et al., 2018).

Gut Inflammation Is Attenuated in GzmA-Deficient (KO) Mice

To address whether GzmA also regulates the gut inflammatory response in the absence of CRC, we induced DSS colitis without AOM. As shown in Figure 5A, WT mice displayed a pronounced reduction of body weight in the first week after DSS treatment. Weight loss was significantly attenuated in GzmA^{KO} mice (Figure 5A). The severity of colitis in GzmA^{KO} mice was also significantly decreased compared with WT mice, as indicated by the clinical score (Figure 5A). Attenuated weight loss and reduced clinical regression resulted in a significant increase in survival of GzmA^{KO} mice relative to WT mice (Figure 5B). During DSS-induced colitis, most WT mice died during the acute phase; thus, later on, the differences between WT and GzmA^{KO} were less pronounced in terms of clinical score and weight loss. In addition, once animals entered the chronic phase, the disease severity was reduced macroscopically (score and weight); thus, the differences were attenuated.

Next, we analyzed the pathological changes observed in colon tissue during DSS-induced colitis and compared these with DSS/AOM-treated animals. As shown in Figure 5C, we found significant shortening in colon length and increased wet weight in WT mice relative to GzmA^{KO} mice. Both colon length reduction and weight increase are common changes observed during colitis. The inflammatory macroscopic score was significantly lower in GzmA^{KO} mice than in WT mice. Histological microscopic examination (Figure 5D) was consistent with the macroscopic colitis and clinical score. DSS-treated WT mice showed leukocyte infiltration in the lamina propria, epithelial hyperplasia, and the presence of markers of severe inflammation, such as crypt abscesses, submucosal inflammation, and ulcers. By contrast, GzmA^{KO} mice showed fewer signs of inflammation and mucosal injury. The inflammatory infiltrate in the colon of GzmA^{KO} mice only affected superficial layers of the mucosa, whereas the crypts were more preserved. Individual parameters and total histological score (the sum of all individual parameters) were both significantly lower in GzmA^{KO} mice than in WT mice.

Similar results were found in DSS/AOM-treated mice, although in this case, the severity and disease scores are reduced in comparison with DSS-treated animals (Figure S6).

Inflammatory Cytokines Are Reduced in Gut from GzmA^{KO} Mice during Acute and Chronic Inflammation

A role for GzmA in gut inflammation was confirmed when analyzing the generation of proinflammatory cytokines in CR tissue from DSS-treated animals. In acute colitis (Figure S7A), all

(C) Group of DSS/AOM-treated mice were sacrificed at day 28, and colon tissue sections were stained with antibodies to vimentin, β-catenin, SNAIL-1, and Ki-67. Scale bars, 100 μm.

(D) Graphs representing the percentage of Ki-67-positive nuclei and the number of positive cells per field for SNAIL-1 and vimentin among all crypt cells. Analyses were performed by quantifying all cells in five random fields per tissue slide (3 slides per animal), as indicated in STAR Methods. Data are presented as mean ± SEM from at least 5 biological replicates (individual mice). Statistical analyses were performed by unpaired t test. *$p < 0.05$; ***$p < 0.001$.

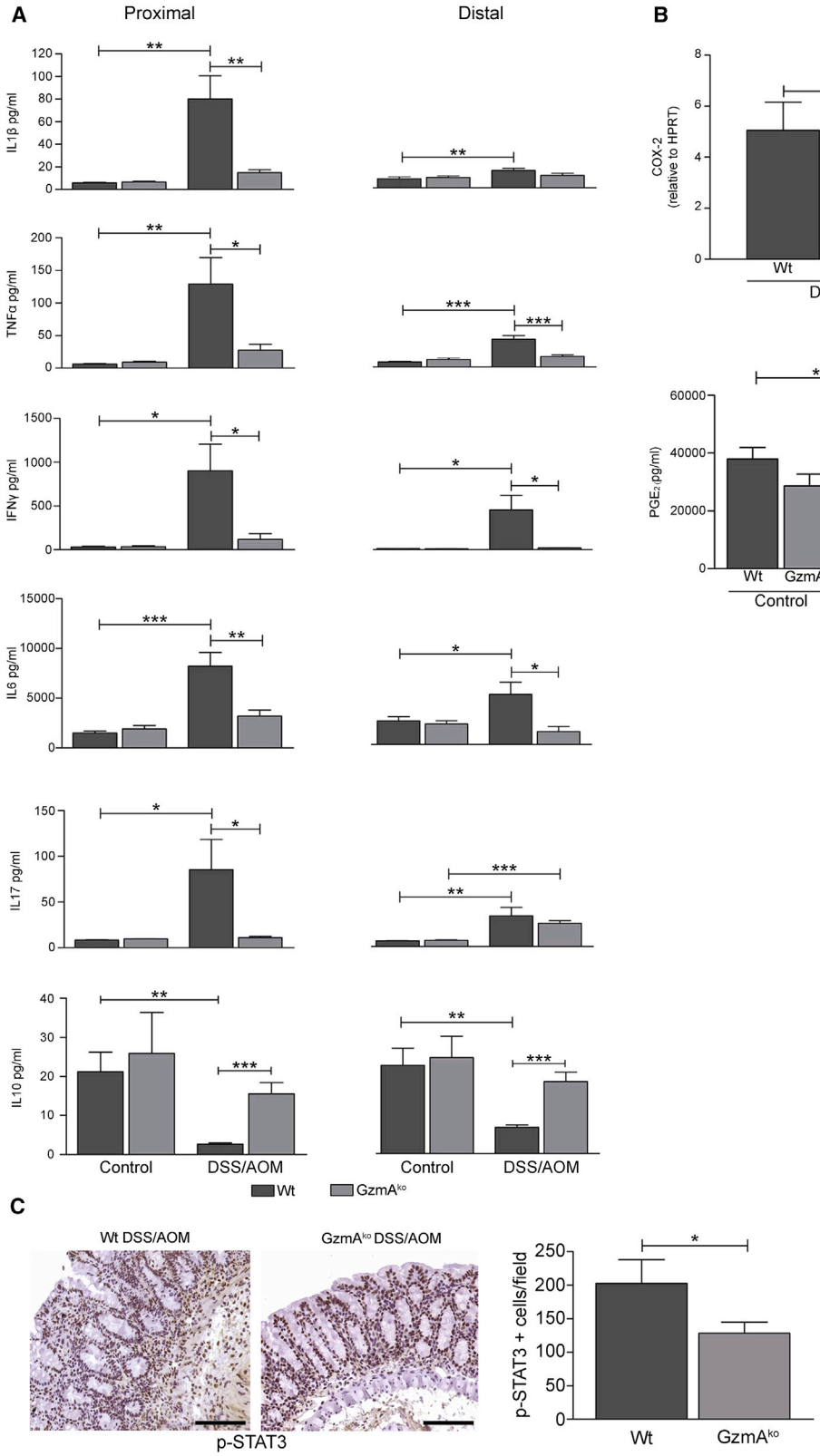

(legend on next page)

cytokines tested were significantly increased in WT animals compared with GzmA^{KO} mice, in both proximal and distal colon, except for IL-6. As expected, we found lower levels of IL-10 in DSS-treated animals compared with untreated healthy animals, without significant differences between WT and KO strains. However, IL-10 levels were slightly higher in GzmA^{KO} than in WT mice during DSS-induced colitis. The level of IL-10 was only significantly reduced by DSS treatment in proximal colon tissue from WT mice.

During chronic colitis, all inflammatory cytokines were also significantly reduced in GzmA^{KO} mice relative to WT mice in both proximal and distal colon (Figure S7B). None of the cytokines significantly increased in DSS-treated GzmA^{KO} mice. In contrast to proinflammatory cytokines, the level of IL-10 was significantly decreased in WT mice compared with GzmA^{KO} mice, in both proximal and distal colon.

The steady-state level of inflammatory cytokines in untreated mice (Figure 4A; Figure S7) is similar in WT and GzmA^{KO} groups, indicating that basal differences in colon integrity do not contribute to the attenuation of inflammation and CRC development in GzmA^{KO} mice. Confirming this assumption, baseline intestinal permeability was not different between WT and GzmA^{KO} mice (Figure S2C).

Altogether, the results employing the intestinal inflammatory model confirm the role of GzmA in modulating gut inflammation and CRC development *in vivo*.

Extracellular GzmA Induces IL-6 Production in M1 Macrophages by NF-κB, which Is Not Affected by COX-2 or Inflammasome Inhibition

As shown earlier, several proinflammatory cytokines were significantly reduced in GzmA^{KO} animals in comparison with WT animals during CRC and colitis *in vivo* (Figure 4A; Figure S7). In addition, active GzmA was present in supernatants from *ex vivo* colon cultures. Thus, we addressed whether extracellular GzmA can induce the production of proinflammatory cytokines in primary M1 macrophages, focusing in those known to be produced by this cell type: IL-6, TNF-α, and IL-1β. As shown in Figure S2E, GzmA significantly induced the expression of IL-6 and TNF-α in macrophages. In contrast, IL-1β was not induced by GzmA. Lipopolysaccharide (LPS) significantly enhanced the generation of all cytokines. Our results suggest that GzmA is able to induce an inflammatory cytokine response *in vitro* with a specific increase in IL-6 and TNF-α. Because of the complexity of the networks involved in cytokine expression and specially in the context of *in vivo* inflammatory responses, we focused our efforts to analyze the mechanism involved in IL-6 production, a cytokine that plays a key negative role in the regulation of CRC development in both humans and mice.

As shown in Figure 6A, GzmA-mediated induction of IL-6 was markedly reduced in the presence of the GzmA-specific inhibitor serpinb6b (Kaiserman et al., 2014) and was not reproduced with inactivated GzmA, confirming that GzmA induces IL-6 production by a mechanism involving proteolysis.

As shown in Figure 6B, the specific NF-κB inhibitor celastrol abrogated IL-6 production mediated by GzmA. As expected, celastrol also inhibited IL-6 production induced by LPS, confirming the efficacy of the inhibitor to block NF-κB-dependent cytokine production. In contrast, IL-6 production was not affected by the COX-2 inhibitor celecoxib or the caspase-1 inhibitor VX-765 (Figure 6B), suggesting that the regulation of IL-6 by GzmA during DSS/AOM-induced tumorigenesis is independent of COX-2 and inflammasome/caspase-1 activity. Extracellular GzmA did not affect macrophage viability (Figure 6C), suggesting that generation of IL-6 was not a consequence of the release of cell debris or other molecules as a consequence of macrophage cell death.

IL-6 production in response to GzmA was undiminished in macrophages deficient in either protease-activated receptor 1 (PAR1) or PAR2 (Figure S2F). Thus, these results do not support for a role of these receptors during GzmA-mediated inflammation in macrophages.

Next, we determined whether the IL-6 induced by GzmA in macrophages promotes the activation of pSTAT3 in the MC-38 cell line (Figure 6D). As expected, IL-6 increased the expression of pSTAT3 that was inhibited by a blocking anti-IL-6 antibody. Similarly, the stimulation of MC-38 cells with supernatant of macrophages previously stimulated with recombinant mouse GzmA increased the phosphorylation of STAT3, which was prevented by blocking IL-6. Stimulation of MC-38 with supernatants from macrophages stimulated with LPS, a potent IL-6 inductor, also increased the expression of pSTAT3 (Figure 6D). Direct stimulation of MC-38 cells with recombinant mouse GzmA did not increase the expression of pSTAT3 (Figure 6D; Figure S2D). These results argue that reduced pSTAT3 in colonic tissue from GzmA-deficient DSS/AOM-treated mice (Figure 4C) is secondary to the reduction in IL-6 production in these mice.

Figure 4. GzmA Deficiency Attenuates Colon Inflammation during CRC Development Induced by DSS/AOM

CRC was induced in male C57BL/6 WT and GzmA^{KO} mice, as described in STAR Methods, which were sacrificed at day 56 with colonic tissue samples (30 mg) cultured during 24 h.

(A) Supernatant was collected and the levels of IL-1β, TNF-α, IFN-γ, IL-6, IL-17, and IL-10 were quantified by ELISA in proximal and distal colon. Data are presented as mean ± SEM from at least 10 biological replicates performed in 4 independent experiments. Statistical analyses were performed by one-way ANOVA test with Bonferroni's post-test. *$p < 0.05$; **$p < 0.01$; ***$p < 0.001$.

(B) mRNA levels of *COX-2* were determined by qRT-PCR (normalized to the amount of *HPRT* mRNA). Data are presented as mean ± SEM from 4 biological replicates (individual mice) performed in 2 independent experiments. Statistical analyses were performed by unpaired t test. *$p < 0.05$. Levels of PGE_2 were quantified by ELISA in *ex vivo* culture of colonic tissue. Data are presented as mean ± SEM from at least 10 biological replicates (individual mice) performed in 4 independent experiments. Statistical analyses were performed by one-way ANOVA test with Bonferroni's post-test. **$p < 0.01$.

(C) Group of mice were sacrificed at day 28, and colon tissue sections were stained with antibodies to pSTAT3. Scale bars, 100 μm. The graph represents the number of positive cells per field for pSTAT3 among all crypt cells. Analyses were performed by quantifying all cells in five random fields per tissue slide (3 slides per animal), as indicated in STAR Methods. Data are presented as mean ± SEM from at least 5 biological replicates (individual mice). Statistical analyses were performed by unpaired t test. *$p < 0.05$.

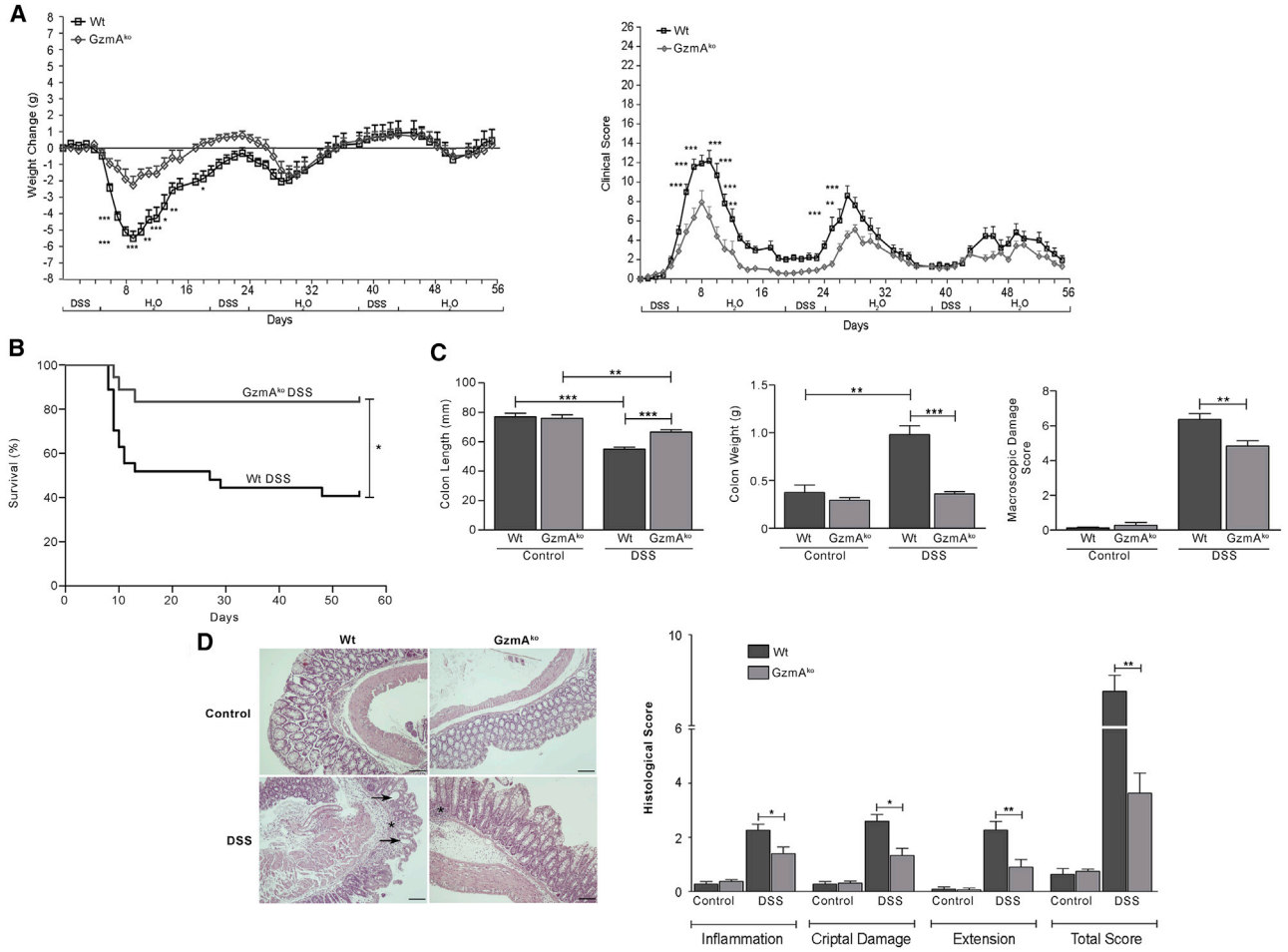

Figure 5. DSS-Induced Colitis and Macroscopic and Microscopic Damage Are Attenuated in GzmA-Deficient Mice

Male C57BL/6 WT and GzmA^{KO} mice were treated with DSS, as described in STAR Methods.

(A) Changes in weight and clinical score were evaluated every 1–2 days. Data are presented as mean ± SEM of 33 (WT) and 26 (GzmA^{KO}) biological replicates (individual mice) performed in 4 independent experiments. Statistical analyses were performed by two-way ANOVA test with Bonferroni's post-test. *$p < 0.05$; **$p < 0.01$; ***$p < 0.001$.

(B) Survival curves corresponding to 33 (WT) and 26 (GzmA^{KO}) biological replicates (individual mice) performed in 4 independent experiments. Statistical analyses were performed by log rank test. *$p < 0.05$.

(C) At the end of the study, the animals were sacrificed, the colon was measured and weighed, and the visible colon damage was scored, as described in STAR Methods. Data are presented as mean ± SEM of 33 (WT) and 26 (GzmA^{KO}) biological replicates (individual mice) in 4 independent experiments. Statistical analyses were performed by one-way ANOVA test with Bonferroni's post-test. **$p < 0.01$; ***$p < 0.001$.

(D) Colonic tissues were removed and processed for histopathology, as described in Method Details. Representative pictures are shown in the left panels. Scale bar, 100 μm. Asterisks indicate inflammation, and arrows show hypertrophic lymphatic vessels in DSS-treated mice. A histological score was established, as indicated in Method Details. The right graph represents the score of each parameter and the total score. Data are presented as mean ± SEM of 5 (WT and GzmA^{KO}) biological replicates (individual mice). Statistical analyses were performed by one-way ANOVA test with Bonferroni's post-test. *$p < 0.05$; **$p < 0.01$.

Therapeutic GzmA Inhibition Reduces CRC Development

Finally, we decided to evaluate whether therapeutic inhibition of GzmA in WT mice with established gut inflammation would attenuate inflammation and prevent CRC progression. Thus, WT mice were treated with the inhibitor serpinb6b 35 days after DSS/AOM treatment, when the intestinal barrier was already disrupted and EMT and colon dysplasia were initiated. As shown in Figure 7A, the levels of IL-6 and TNF-α in supernatants from explant cultures was significantly reduced in WT mice treated with serpinb6b in both distal and proximal colon, suggesting that extracellular GzmA drives inflammation in DSS/AOM-treated animals. No reduction was observed with an inactive serpinb6b. The reduction in macroscopic colon damage obtained with serpinb6b treatment was similar to that observed with genetic GzmA deficiency (Figure 7B). Notably, serpinb6b treatment also significantly reduced the incidence and the number of tumors in DSS/AOM-treated WT mice (Figure 7B), confirming that therapeutic inhibition of extracellular GzmA reduces inflammatory CRC.

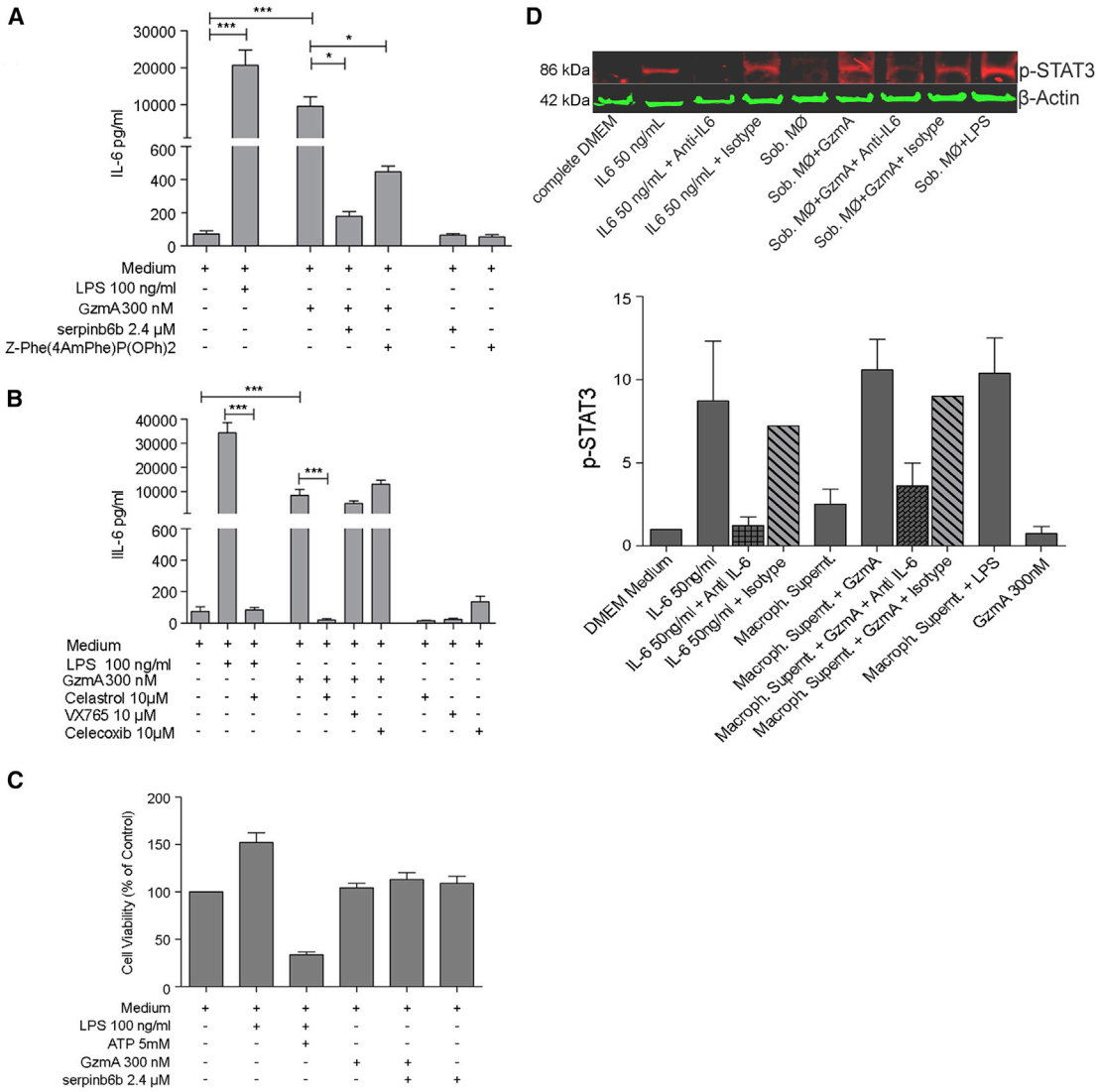

Figure 6. Extracellular GzmA Induces IL-6 Production by Macrophages and Promotes Activation of STAT3

(A) Bone-marrow-derived M1 macrophages were stimulated with active GzmA (300 nM) or GzmA inactivated with serpinb6b, a specific inhibitor of mouse GzmA.

(B) Macrophages were treated with specific inhibitors of NF-κB (celastrol), COX-2 (celecoxib), or caspase-1 (VX-765) during the 1 h before the addition of GzmA (300 nM). As positive control, macrophages were stimulated with *E. coli* LPS (100 ng/mL). Macrophages were incubated for 24 h at 37°C and 5% CO_2, supernatants were collected, and the levels of IL-6 were measured by ELISA. Data are presented as mean ± SEM from two independent experiments performed by triplicates. Statistical analyses were performed by one-way ANOVA test with Bonferroni's post-test. *$p < 0.05$; ***$p < 0.001$.

(C) PrestoBlue cell viability of macrophages stimulated with active GzmA (300 nM), GzmA inactivated with serpinb6b, 100 ng/mL *E. coli* LPS, or 100 ng/mL *E. coli* LPS with 5 mM ATP for 24 h.

(D) Western blot of MC-38 cells incubated with mouse IL-6 (50 ng/mL) (as positive control), supernatant from recombinant mouse GzmA-stimulated macrophage (300 nM), or supernatant from LPS-stimulated macrophage (100 ng/mL). Supernatant from unstimulated macrophage, supernatant from recombinant mouse GzmA-stimulated macrophage treated with mAb IL-6 or isotype (BioXCell), and supernatant from mouse IL-6 treated with mAb IL-6 or isotype (BioXCell) were added as control. The cells were stimulated with the indicated stimuli for 15 min, after which cells were lysed and western blotted using pSTAT3 antibody (Tyr705). IL-6-dependent changes in STAT3 phosphorylation were evaluated by quantifying band intensities on pSTAT3 blots and comparing to β-actin band intensities as a loading control, with the aid of ImageJ software (lower graph).

DISCUSSION

If not properly regulated, inflammatory mechanisms involved in host defense and cancer immunosurveillance can promote cancer development, progression, and resistance to treatment. The best example of this dichotomy is CRC (Crusz and Balkwill, 2015; Erreni et al., 2011; Shalapour and Karin, 2015), the second-most deadly of all cancers. Here we identify extracellular GzmA as a new mechanism by which the immune system can facilitate CRC development, thus contributing to understanding of the molecular mechanism underlying this pathology and opening a new therapeutic opportunity.

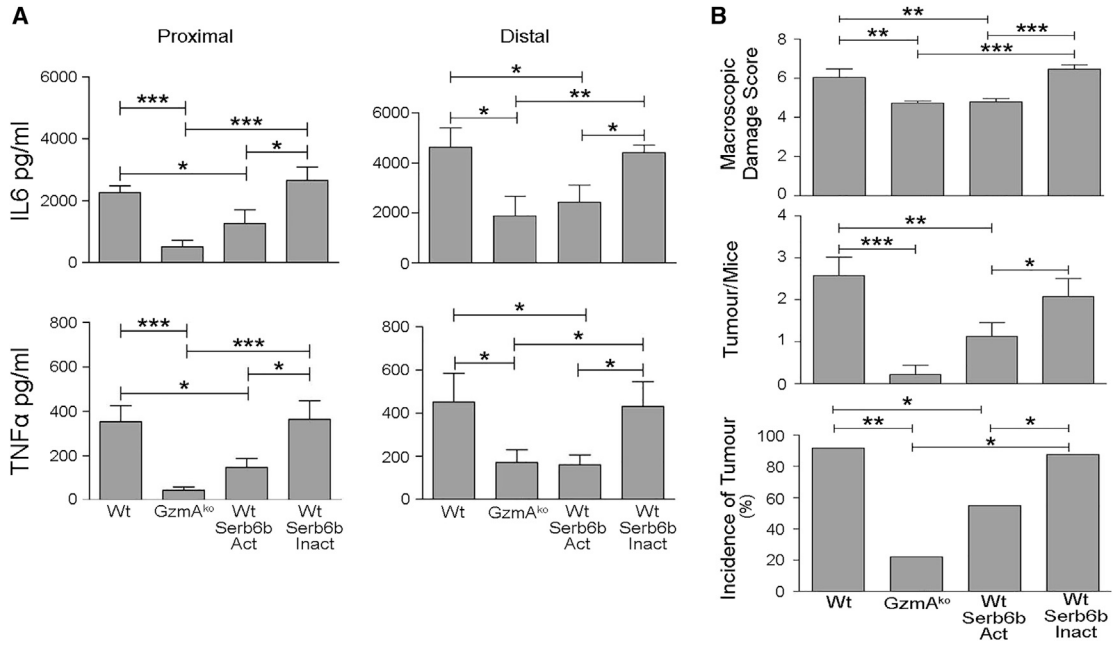

Figure 7. A Macromolecular GzmA Inhibitor Reduces CRC and Colon Inflammation in DSS/AOM-Treated WT Mice

CRC was induced in male C57BL/6 WT and GzmA^{KO} mice with AOM, as described in STAR Methods. On day 35, a group of mice was treated with five doses of serpinb6b (20 μg intravenously [i.v.]) every other day. Mice were sacrificed at day 50. As control, a group of mice was treated with inactivated serpinb6b.

(A) Colonic tissue samples (30 mg) were cultured during 24 h, supernatant was collected, and the levels of IL-6 and TNF-α were quantified by ELISA in proximal and distal colon.

(B) Macroscopic colon damage score, number of tumors, and incidence of tumors. Data are presented as mean ± SEM from at least 10 biological replicates (individual mice) performed in 3 independent experiments. Statistical analyses were performed by one-way ANOVA test with Bonferroni's post-test. *$p < 0.05$; **$p < 0.01$; ***$p < 0.001$.

GzmA belongs to a family of serine proteases traditionally recognized as anti-tumor and anti-infective agents because of the ability to trigger cell death on target cells *in vitro*. Challenging this dogma, we now show that GzmA plays a critical role in promoting gut inflammation and thereby tumor development. This effect correlates with the ability of extracellular GzmA to promote NF-κB-dependent IL-6 production in macrophages, which in turn, results in IL-6-dependent pSTAT3 activation in CRC cells. Although several inflammatory molecules have been shown to modulate the different stages of epithelial cell transformation and CRC development, our combined *in vitro* and *in vivo* data indicate that GzmA-induced IL-6 production may provide an important link between immune cell infiltration and activation of STAT3 and other protumorigenic pathways during CRC development. This does not exclude that other mechanisms could link GzmA to inflammation and CRC development, such as modulation of intestinal permeability or proteolytic release of inflammatory damage-associated molecular patterns (DAMPs) from intestinal cells. GzmB has been reported to release peptides with proinflammatory activity derived from the extracellular matrix (Turner et al., 2019).

The data showing that therapeutic inhibition of GzmA by serpinb6b represent a proof of concept that GzmA is a potential therapeutic target in CRC. These results are not directly translatable, because serpinb6b does not block human GzmA. Antithrombin III (SerpinC1) is an endogenous inhibitor of human GzmA (Masson and Tschopp, 1988) that is reduced during CRC (Peltier et al., 2016). Supporting the translational relevance of our findings, our analysis of human CRC patients shows strong correlation between *GZMA* expression and inflammatory score.

Importantly, the conclusions arising from study of GzmA-deficient animals were confirmed by employing an extracellular GzmA inhibitor in WT mice, negating the argument that protection is related to the presence of an existing colonic phenotype in GzmA^{KO} animals at baseline that might be driving a DSS-protective phenotype. Strengthening this conclusion, we show that microbiota composition, inflammatory cytokine levels, and intestinal permeability at steady state are identical in WT and in GzmA^{KO} mice. Moreover, the extracellular GzmA inhibitor, serpinb6b, was effective when inoculated at 5 weeks, indicating that the loss of intestinal barrier during DSS/AOM treatment can be dissociated from the effect of GzmA on CRC development. GzmA is the first member of the Gzms family shown to promote gut inflammation and CRC development. GzmM has been reported to protect against colitis and CRC in the DSS/AOM model (Souza-Fonseca-Guimaraes et al., 2016), suggesting that therapeutic approaches would need to be specific for GzmA. We did not find significant expression of *GZMM* in transcriptomics analysis of two cohorts of human CRC samples (data not shown). *GZMK* and *GZMH* expression also correlated with inflammatory score but at lower abundance than *GZMA* (data not shown).

The role of inflammation has been widely studied during tumor development, although the molecular mechanisms involved have not been completely elucidated. Thus, until now, the balance between beneficial and deleterious effects of inflammation (host protection versus tumor development/progression) has not been well understood. Most molecules identified as protumor inflammatory factors are also critically involved in protection, with the notable exception of COX-2. Thus, manipulation of inflammation is difficult to achieve during cancer treatment without risking adverse effects, including opportunistic infections (Rose-John et al., 2017; Salvana and Salata, 2009). Previous results from us and others have shown that GzmA^{KO} mice efficiently clear experimental viral and bacterial infections, as well as tumors (Anthony et al., 2010a; Arias et al., 2014; Trapani and Smyth, 2002). Thus, GzmA inactivation should not predispose a patient to major side effects including infection and cancer, unlike other common anti-inflammatory drugs, like IL-6 or TNF-α blockers (Rose-John et al., 2017; Salvana and Salata, 2009).

Our study has identified GzmA as a potential target to treat CRC, and our data suggest that its potential effects are mainly mediated at the extracellular level. The cellular sources responsible for GzmA secretion and CRC development remain to be defined. High levels of infiltrating lymphocytes expressing GzmA have been previously found in humans with UC (Müller et al., 1998), and patients expressing high levels of *GZMA* in CD4$^+$integrin-αE$^+$ cells had a better response to anti-inflammatory immunotherapy with a monoclonal antibody (mAb) against the β7-integrin subunit (etrolizumab) (Tew et al., 2016). Reflecting the situation in UC patients, we have found that conventional CD8$^+$/CD3$^+$ T cells, CD8$\alpha\alpha^+$ lymphocytes, and NK/ILC1 cells increase in the intestinal tissue of mice treated with DSS/AOM. However, in contrast to the previously mentioned studies, GzmA expression was mainly associated with CD8$^+$ lymphocytes, NK cells, and NKT cells, but not with CD4$^+$ T cells, indicating that the mechanism by which GzmA contributes to UC and CRC might be different. It is plausible that some of these cells could secrete GzmA after activation of specific pattern recognition receptors (PRRs) in response to extracellular microbe-derived components present in the colon (reviewed in Souza-Fonseca-Guimaraes et al., 2012). This hypothesis will be difficult to test, because depletion of NK/NKT or CD8$^+$ cells would be expected to modulate tumor progression independent of GzmA. There have been no previous studies investigating GzmA expression in CRC patients. In agreement with the results in the mouse model, we have found a clear correlation between *GZMA* and inflammation in two independent datasets comprising human tumors with different clinical and molecular characteristics. No such correlation exists between *GZMB* and inflammation. Although this does not necessarily imply a causal role of *GZMA* expression in inflammation, the combined results in mouse and human models strongly suggest a role for GzmA in regulating inflammation during CRC. We also analyzed whether GzmA could have a prognostic value in CRC patients but did not find correlation between *GZMA* expression and prognosis (measured as time to recurrence or overall survival) in our Colonomics database or in larger public databases (GEO: GSE39582 or the Human Protein Atlas). These results suggest that GzmA would have a prominent role in the first stages of CR carcinogenesis, but once macroscopic tumors have been developed, other molecules would be more relevant for cancer progression. Supporting this hypothesis, other factors known to critically contribute to CRC development, such IL-6 or Cox-2, did not show prognostic value in the databases indicated earlier, suggesting that like GzmA, these molecules might contribute to cancer initiation, rather than progression. Indeed, recent data indicate that Th1-related inflammation in human cancer, including CRC, is a protective factor once tumors are established, suggesting that the detrimental effects of inflammation during tumor initiation might have opposing role once tumors are established (Ponzetta et al., 2019).

A key to understanding the carcinogenic mechanism activated by GzmA, and hence to therapeutically targeting this enzyme, is the location of its proinflammatory action—specifically, whether GzmA-induced inflammation requires intracellular delivery by perforin or whether it can be triggered from the extracellular space. We showed that active GzmA is present in the supernatant of colon explant cultures *ex vivo* and that *in vivo* inactivation of GzmA by exogenous serpinb6b reduces inflammation and CRC incidence. We additionally showed that extracellular active GzmA induces the expression of IL-6 in M1 macrophages, which have been linked to CRC in humans (Shabo et al., 2014) and DSS/AOM-treated mice (Wang et al., 2015), in a process inhibited by NF-κB inactivation. Supporting our data in mice, we have previously found that extracellular active GzmA induces the generation of IL-6 in non-primed human macrophages (Metkar et al., 2008), although the mechanisms underlying this process are unknown. Thus, all our results support that GzmA exerts its proinflammatory carcinogenic function from the extracellular space, a key finding to design therapeutic approaches to block GzmA activity. In summary, GzmA constitutes a new molecular mechanism that contributes to CRC development *in vivo* by regulating gut inflammatory responses using mechanisms that sustain the perpetuation of an inflammatory microenvironment, probably by its action on tissue macrophages. Therapeutic inhibition of extracellular GzmA reduces inflammation and tumor number and incidence, suggesting that the development of effective GzmA inhibitors could have a beneficial effect in the treatment of gut inflammation and CRC development in a more selective and safer way than other therapies commonly used in the treatment of these diseases.

STAR★METHODS

Detailed methods are provided in the online version of this paper and include the following:

- KEY RESOURCES TABLE
- RESOURCE AVAILABILITY
  - Lead Contact
  - Materials Availability
  - Data and Code Availability
- EXPERIMENTAL MODEL AND SUBJECT DETAILS
  - Human samples
  - Mice
  - Cells lines and primary cell cultures

SUPPLEMENTAL INFORMATION

Supplemental Information can be found online at https://doi.org/10.1016/j.celrep.2020.107847.

ACKNOWLEDGMENTS

This work was supported in part by FEDER/Gobierno de Aragón (group B29), Ministerio de Economia y Competitividad (SAF2014-54763-C2-1 and SAF2017-83120-C2-1-R to J.P. and SAF2014-54763-C2-2-R to E.M.G.), and Instituto de Salud Carlos III (PI13/00864 to L.M.-L.). Predoctoral grants/contracts from Fundacion Santander/Universidad de Zaragoza (to L.S. and M.A.A.), Gobierno de Aragon (to I.U.-M., L.C., L.S., and P.J.-S.), and FPU/Ministerio de Educación, Cultura y Deportes (to P.M.L.). I.U.-M. was supported by Fondo Garantía Empleo Juvenil/INAEM. M.A.A. has a Juan de la Cierva contract (Ministerio de Ciencia, Innovación y Universidades). J.P. was supported by Fundación Aragon I+D (ARAID). The authors acknowledge the use of Servicios Científico Técnicos del CIBA (IACS-Universidad de Zaragoza) and Servicios Apoyo Investigación de la Universidad de Zaragoza.

AUTHOR CONTRIBUTIONS

J.P. and M.A.A. conceived the original idea. J.P. and M.A.A. coordinated the study. J.P., M.A.A., L.S., M.C., L.M.-L., V.M., S.M., A.F., G.G.-G., R.P., R.d.C., E.M.G., A.A., P.P., and E.C. designed the research studies. L.S., M.A.A., M.C., M.G.T., M.G., E.L., G.M., J.A.U., R.d.C., M.G., P.M.L., L.C., and I.U.-M. conducted experiments. L.S., M.C., V.M., M.G.T., M.G., E.L., R.P., L.M.-L., M.G., P.M.L., L.C., I.U.-M., G.M., J.A.U., E.M.G., A.A., and A.F. acquired and analyzed data. E.T. supervised and designed animal experiments. R.S.-P. performed and analyzed all experimental work concerning the human transcriptome. P.P., E.C., and P.I.B. provided key research reagents. L.S. wrote the first version of the manuscript. M.C., L.M.-L., S.M., A.F., G.G.-G., R.d.C., E.M.G., P.I.B., and R.S.-P. wrote the manuscript. L.S., M.A.A., and J.P. wrote the final version of the manuscript.

DECLARATION OF INTERESTS

The authors declare no competing interests.

Received: October 14, 2019
Revised: February 11, 2020
Accepted: June 11, 2020
Published: July 7, 2020

REFERENCES

Afonina, I.S., Cullen, S.P., and Martin, S.J. (2010). Cytotoxic and non-cytotoxic roles of the CTL/NK protease granzyme B. Immunol. Rev. *235*, 105–116.

Anthony, D.A., Andrews, D.M., Chow, M., Watt, S.V., House, C., Akira, S., Bird, P.I., Trapani, J.A., and Smyth, M.J. (2010a). A role for granzyme M in TLR4-driven inflammation and endotoxicosis. J. Immunol. *185*, 1794–1803.

Anthony, D.A., Andrews, D.M., Watt, S.V., Trapani, J.A., and Smyth, M.J. (2010b). Functional dissection of the granzyme family: cell death and inflammation. Immunol. Rev. *235*, 73–92.

Arias, M.A., Jiménez de Bagües, M.P., Aguiló, N., Menao, S., Hervás-Stubbs, S., de Martino, A., Alcaraz, A., Simon, M.M., Froelich, C.J., and Pardo, J. (2014). Elucidating sources and roles of granzymes A and B during bacterial infection and sepsis. Cell Rep. *8*, 420–429.

Arias, M., Martínez-Lostao, L., Santiago, L., Ferrandez, A., Granville, D.J., and Pardo, J. (2017). The Untold Story of Granzymes in Oncoimmunology: Novel Opportunities with Old Acquaintances. Trends Cancer *3*, 407–422.

Bernstein, C.N., Blanchard, J.F., Kliewer, E., and Wajda, A. (2001). Cancer risk in patients with inflammatory bowel disease: a population-based study. Cancer *91*, 854–862.

Boulard, O., Kirchberger, S., Royston, D.J., Maloy, K.J., and Powrie, F.M. (2012). Identification of a genetic locus controlling bacteria-driven colitis and associated cancer through effects on innate inflammation. J. Exp. Med. *209*, 1309–1324.

Bovenschen, N., and Kummer, J.A. (2010). Orphan granzymes find a home. Immunol. Rev. *235*, 117–127.

Brennan, C.A., and Garrett, W.S. (2016). Gut Microbiota, Inflammation, and Colorectal Cancer. Annu. Rev. Microbiol. *70*, 395–411.

Chowdhury, D., and Lieberman, J. (2008). Death by a thousand cuts: granzyme pathways of programmed cell death. Annu. Rev. Immunol. *26*, 389–420.

Crusz, S.M., and Balkwill, F.R. (2015). Inflammation and cancer: advances and new agents. Nat. Rev. Clin. Oncol. *12*, 584–596.

De Robertis, M., Massi, E., Poeta, M.L., Carotti, S., Morini, S., Cecchetelli, L., Signori, E., and Fazio, V.M. (2011). The AOM/DSS murine model for the study of colon carcinogenesis: From pathways to diagnosis and therapy studies. J. Carcinog. *10*, 9.

Eaden, J.A., Abrams, K.R., and Mayberry, J.F. (2001). The risk of colorectal cancer in ulcerative colitis: a meta-analysis. Gut *48*, 526–535.

Ericsson, A.C., Gagliardi, J., Bouhan, D., Spollen, W.G., Givan, S.A., and Franklin, C.L. (2018). The influence of caging, bedding, and diet on the composition of the microbiota in different regions of the mouse gut. Sci. Rep. *8*, 4065.

Erreni, M., Mantovani, A., and Allavena, P. (2011). Tumor-associated Macrophages (TAM) and Inflammation in Colorectal Cancer. Cancer Microenviron. *4*, 141–154.

Fearon, E.R., and Vogelstein, B. (1990). A genetic model for colorectal tumorigenesis. Cell *61*, 759–767.

Fichtner-Feigl, S., Kesselring, R., and Strober, W. (2015). Chronic inflammation and the development of malignancy in the GI tract. Trends Immunol. *36*, 451–459.

Francí, C., Takkunen, M., Dave, N., Alameda, F., Gómez, S., Rodríguez, R., Escrivà, M., Montserrat-Sentís, B., Baró, T., Garrido, M., et al. (2006). Expression of Snail protein in tumor-stroma interface. Oncogene *25*, 5134–5144.

Galon, J., Pagès, F., Marincola, F.M., Angell, H.K., Thurin, M., Lugli, A., Zlobec, I., Berger, A., Bifulco, C., Botti, G., et al. (2012). Cancer classification using the Immunoscore: a worldwide task force. J. Transl. Med. *10*, 205.

Glocker, E.O., Kotlarz, D., Klein, C., Shah, N., and Grimbacher, B. (2011). IL-10 and IL-10 receptor defects in humans. Ann. N Y Acad. Sci. *1246*, 102–107.

Granville, D.J. (2010). Granzymes in disease: bench to bedside. Cell Death Differ. *17*, 565–566.

Guinney, J., Dienstmann, R., Wang, X., de Reyniès, A., Schlicker, A., Soneson, C., Marisa, L., Roepman, P., Nyamundanda, G., Angelino, P., et al. (2015). The consensus molecular subtypes of colorectal cancer. Nat. Med. *21*, 1350–1356.

Han, X., Kitamoto, S., Wang, H., and Boisvert, W.A. (2010). Interleukin-10 overexpression in macrophages suppresses atherosclerosis in hyperlipidemic mice. FASEB J. *24*, 2869–2880.

Izcue, A., Hue, S., Buonocore, S., Arancibia-Cárcamo, C.V., Ahern, P.P., Iwakura, Y., Maloy, K.J., and Powrie, F. (2008). Interleukin-23 restrains regulatory T cell activity to drive T cell-dependent colitis. Immunity *28*, 559–570.

Kaiserman, D., Stewart, S.E., Plasman, K., Gevaert, K., Van Damme, P., and Bird, P.I. (2014). Identification of Serpinb6b as a species-specific mouse granzyme A inhibitor suggests functional divergence between human and mouse granzyme A. J. Biol. Chem. *289*, 9408–9417.

Kaler, P., Godasi, B.N., Augenlicht, L., and Klampfer, L. (2009). The NF-κB/AKT-dependent Induction of Wnt Signaling in Colon Cancer Cells by Macrophages and IL-1β. Cancer Microenviron. *2*, 69–80.

Kalluri, R., and Weinberg, R.A. (2009). The basics of epithelial-mesenchymal transition. J. Clin. Invest. *119*, 1420–1428.

Karin, M. (1998). The NF-kappa B activation pathway: its regulation and role in inflammation and cell survival. Cancer J. Sci. Am. *4* (*Suppl 1*), S92–S99.

Kirchberger, S., Royston, D.J., Boulard, O., Thornton, E., Franchini, F., Szabady, R.L., Harrison, O., and Powrie, F. (2013). Innate lymphoid cells sustain colon cancer through production of interleukin-22 in a mouse model. J. Exp. Med. *210*, 917–931.

Kühn, R., Löhler, J., Rennick, D., Rajewsky, K., and Müller, W. (1993). Interleukin-10-deficient mice develop chronic enterocolitis. Cell *75*, 263–274.

Lasry, A., Zinger, A., and Ben-Neriah, Y. (2016). Inflammatory networks underlying colorectal cancer. Nat. Immunol. *17*, 230–240.

Li, Y., and Laterra, J. (2012). Cancer stem cells: distinct entities or dynamically regulated phenotypes? Cancer Res. *72*, 576–580.

Mantovani, A. (2018). The inflammation—cancer connection. FEBS J. *285*, 638–640.

Marisa, L., de Reyniès, A., Duval, A., Selves, J., Gaub, M.P., Vescovo, L., Etienne-Grimaldi, M.C., Schiappa, R., Guenot, D., Ayadi, M., et al. (2013). Gene expression classification of colon cancer into molecular subtypes: characterization, validation, and prognostic value. PLoS Med. *10*, e1001453.

Martin, P., Wallich, R., Pardo, J., Müllbacher, A., Munder, M., Modolell, M., and Simon, M.M. (2005). Quiescent and activated mouse granulocytes do not express granzyme A and B or perforin: similarities or differences with human polymorphonuclear leukocytes? Blood *106*, 2871–2878.

Martínez-Lostao, L., Anel, A., and Pardo, J. (2015). How Do Cytotoxic Lymphocytes Kill Cancer Cells? Clin. Cancer Res. *21*, 5047–5056.

Masson, D., and Tschopp, J. (1988). Inhibition of lymphocyte protease granzyme A by antithrombin III. Mol. Immunol. *25*, 1283–1289.

Matheus, N., Mendoza, C., Iceta, R., Mesonero, J.E., and Alcalde, A.I. (2009). Regulation of serotonin transporter activity by adenosine in intestinal epithelial cells. Biochem. Pharmacol. *78*, 1198–1204.

Metkar, S.S., Menaa, C., Pardo, J., Wang, B., Wallich, R., Freudenberg, M., Kim, S., Raja, S.M., Shi, L., Simon, M.M., and Froelich, C.J. (2008). Human and mouse granzyme A induce a proinflammatory cytokine response. Immunity *29*, 720–733.

Montonye, D.R., Ericsson, A.C., Busi, S.B., Lutz, C., Wardwell, K., and Franklin, C.L. (2018). Acclimation and Institutionalization of the Mouse Microbiota Following Transportation. Front. Microbiol. *9*, 1085.

Müller, S., Lory, J., Corazza, N., Griffiths, G.M., Z'graggen, K., Mazzucchelli, L., Kappeler, A., and Mueller, C. (1998). Activated CD4+ and CD8+ cytotoxic cells are present in increased numbers in the intestinal mucosa from patients with active inflammatory bowel disease. Am. J. Pathol. *152*, 261–268.

Neufert, C., Becker, C., and Neurath, M.F. (2007). An inducible mouse model of colon carcinogenesis for the analysis of sporadic and inflammation-driven tumor progression. Nat. Protoc. *2*, 1998–2004.

Olivares-Villagómez, D., and Van Kaer, L. (2018). Intestinal Intraepithelial Lymphocytes: Sentinels of the Mucosal Barrier. Trends Immunol. *39*, 264–275.

Pagès, F., Berger, A., Camus, M., Sanchez-Cabo, F., Costes, A., Molidor, R., Mlecnik, B., Kirilovsky, A., Nilsson, M., Damotte, D., et al. (2005). Effector memory T cells, early metastasis, and survival in colorectal cancer. N. Engl. J. Med. *353*, 2654–2666.

Pardo, J., Wallich, R., Ebnet, K., Iden, S., Zentgraf, H., Martin, P., Ekiciler, A., Prins, A., Müllbacher, A., Huber, M., and Simon, M.M. (2007). Granzyme B is expressed in mouse mast cells *in vivo* and *in vitro* and causes delayed cell death independent of perforin. Cell Death Differ. *14*, 1768–1779.

Pardo, J., Wallich, R., Martin, P., Urban, C., Rongvaux, A., Flavell, R.A., Müllbacher, A., Borner, C., and Simon, M.M. (2008). Granzyme B-induced cell death exerted by *ex vivo* CTL: discriminating requirements for cell death and some of its signs. Cell Death Differ. *15*, 567–579.

Pardo, J., Aguilo, J.I., Anel, A., Martin, P., Joeckel, L., Borner, C., Wallich, R., Müllbacher, A., Froelich, C.J., and Simon, M.M. (2009). The biology of cytotoxic cell granule exocytosis pathway: granzymes have evolved to induce cell death and inflammation. Microbes Infect. *11*, 452–459.

Peltier, J., Roperch, J.P., Audebert, S., Borg, J.P., and Camoin, L. (2016). Quantitative proteomic analysis exploring progression of colorectal cancer: Modulation of the serpin family. J. Proteomics *148*, 139–148.

Ponzetta, A., Carriero, R., Carnevale, S., Barbagallo, M., Molgora, M., Perucchini, C., Magrini, E., Gianni, F., Kunderfranco, P., Polentarutti, N., et al. (2019). Neutrophils Driving Unconventional T Cells Mediate Resistance against Murine Sarcomas and Selected Human Tumors. Cell *178*, 346–360.

Popivanova, B.K., Kitamura, K., Wu, Y., Kondo, T., Kagaya, T., Kaneko, S., Oshima, M., Fujii, C., and Mukaida, N. (2008). Blocking TNF-alpha in mice reduces colorectal carcinogenesis associated with chronic colitis. J. Clin. Invest. *118*, 560–570.

Powell, N., Walker, M.M., and Talley, N.J. (2017). The mucosal immune system: master regulator of bidirectional gut-brain communications. Nat. Rev. Gastroenterol. Hepatol. *14*, 143–159.

Quast, C., Pruesse, E., Yilmaz, P., Gerken, J., Schweer, T., Yarza, P., Peplies, J., and Glöckner, F.O. (2013). The SILVA ribosomal RNA gene database project: improved data processing and web-based tools. Nucleic Acids Res. *41*, D590–D596.

Rose-John, S., Winthrop, K., and Calabrese, L. (2017). The role of IL-6 in host defence against infections: immunobiology and clinical implications. Nat. Rev. Rheumatol. *13*, 399–409.

Salama, P., Phillips, M., Platell, C., and Iacopetta, B. (2011). Low expression of Granzyme B in colorectal cancer is associated with signs of early metastastic invasion. Histopathology *59*, 207–215.

Salvana, E.M., and Salata, R.A. (2009). Infectious complications associated with monoclonal antibodies and related small molecules. Clin. Microbiol. Rev. *22*, 274–290.

Santiago, L., Menaa, C., Arias, M., Martin, P., Jaime-Sánchez, P., Metkar, S., Comas, L., Erill, N., Gonzalez-Rumayor, V., Esser, E., et al. (2017). Granzyme A contributes to inflammatory arthritis in Mice through stimulation of osteoclastogenesis. Arthritis Rheumatol. *69*, 320–334.

Sanz-Pamplona, R., Berenguer, A., Cordero, D., Molleví, D.G., Crous-Bou, M., Sole, X., Paré-Brunet, L., Guino, E., Salazar, R., Santos, C., et al. (2014). Aberrant gene expression in mucosa adjacent to tumor reveals a molecular crosstalk in colon cancer. Mol. Cancer *13*, 46.

Schneider, C.A., Rasband, W.S., and Eliceiri, K.W. (2012). NIH Image to ImageJ: 25 years of image analysis. Nat. Methods *9*, 671–675.

Shabo, I., Olsson, H., Elkarim, R., Sun, X.F., and Svanvik, J. (2014). Macrophage Infiltration in Tumor Stroma is Related to Tumor Cell Expression of CD163 in Colorectal Cancer. Cancer Microenviron. *7*, 61–69.

Shalapour, S., and Karin, M. (2015). Immunity, inflammation, and cancer: an eternal fight between good and evil. J. Clin. Invest. *125*, 3347–3355.

Shenoy, A.K., Fisher, R.C., Butterworth, E.A., Pi, L., Chang, L.J., Appelman, H.D., Chang, M., Scott, E.W., and Huang, E.H. (2012). Transition from colitis to cancer: high Wnt activity sustains the tumor-initiating potential of colon cancer stem cell precursors. Cancer Res. *72*, 5091–5100.

Sobin, L.H., and Compton, C.C. (2010). TNM seventh edition: what's new, what's changed: communication from the International Union Against Cancer and the American Joint Committee on Cancer. Cancer *116*, 5336–5339.

Souza-Fonseca-Guimaraes, F., Adib-Conquy, M., and Cavaillon, J.M. (2012). Natural killer (NK) cells in antibacterial innate immunity: angels or devils? Mol. Med. *18*, 270–285.

Souza-Fonseca-Guimaraes, F., Krasnova, Y., Putoczki, T., Miles, K., MacDonald, K.P., Town, L., Shi, W., Gobe, G.C., McDade, L., Mielke, L.A., et al. (2016). Granzyme M has a critical role in providing innate immune protection in ulcerative colitis. Cell Death Dis. *7*, e2302.

Subramanian, A.R., Weyer-Menkhoff, J., Kaufmann, M., and Morgenstern, B. (2005). DIALIGN-T: an improved algorithm for segment-based multiple sequence alignment. BMC Bioinformatics *6*, 66.

Takahashi, M., Fukuda, K., Sugimura, T., and Wakabayashi, K. (1998). Beta-catenin is frequently mutated and demonstrates altered cellular location in azoxymethane-induced rat colon tumors. Cancer Res. *58*, 42–46.

Tew, G.W., Hackney, J.A., Gibbons, D., Lamb, C.A., Luca, D., Egen, J.G., Diehl, L., Eastham Anderson, J., Vermeire, S., Mansfield, J.C., et al. (2016). Association Between Response to Etrolizumab and Expression of Integrin αE and Granzyme A in Colon Biopsies of Patients With Ulcerative Colitis. Gastroenterology *150*, 477–487.

Trapani, J.A., and Smyth, M.J. (2002). Functional significance of the perforin/granzyme cell death pathway. Nat. Rev. Immunol. *2*, 735–747.

Tuominen, V.J., Ruotoistenmäki, S., Viitanen, A., Jumppanen, M., and Isola, J. (2010). ImmunoRatio: a publicly available web application for quantitative image analysis of estrogen receptor (ER), progesterone receptor (PR), and Ki-67. Breast Cancer Res. *12*, R56.

Turner, C.T., Lim, D., and Granville, D.J. (2019). Granzyme B in skin inflammation and disease. Matrix Biol. *75–76*, 126–140.

Turner, C.T., Zeglinski, M.R., Richardson, K.C., Zhao, H., Shen, Y., Papp, A., Bird, P.I., and Granville, D.J. (2019). Granzyme K Expressed by Classically Activated Macrophages Contributes to Inflammation and Impaired Remodeling. J. Invest. Dermatol. *139*, 930–939.

Voskoboinik, I., Whisstock, J.C., and Trapani, J.A. (2015). Perforin and granzymes: function, dysfunction and human pathology. Nat. Rev. Immunol. *15*, 388–400.

Wang, W., Li, X., Zheng, D., Zhang, D., Peng, X., Zhang, X., Ai, F., Wang, X., Ma, J., Xiong, W., et al. (2015). Dynamic changes and functions of macrophages and M1/M2 subpopulations during ulcerative colitis-associated carcinogenesis in an AOM/DSS mouse model. Mol. Med. Rep. *11*, 2397–2406.

Wensink, A.C., Hack, C.E., and Bovenschen, N. (2015). Granzymes regulate proinflammatory cytokine responses. J. Immunol. *194*, 491–497.

Wirtz, S., Neufert, C., Weigmann, B., and Neurath, M.F. (2007). Chemically induced mouse models of intestinal inflammation. Nat. Protoc. *2*, 541–546.

Yang, L., Yu, H., Dong, S., Zhong, Y., and Hu, S. (2017). Recognizing and managing on toxicities in cancer immunotherapy. Tumour Biol. *39*, 1010428317694542.

Yu, H., Pardoll, D., and Jove, R. (2009). STATs in cancer inflammation and immunity: a leading role for STAT3. Nat. Rev. Cancer *9*, 798–809.

STAR★METHODS

KEY RESOURCES TABLE

REAGENT or RESOURCE	SOURCE	IDENTIFIER
Antibodies		
Anti-p-STAT3 (Tyr705) (Rabbit anti-mouse)	Cell Signaling	Cat# 9145S
Anti-p-NF-κB p65 (Ser536) (Rabbit anti-mouse)	Cell Signaling	Cat# 3000S
Anti-IκBα (44D4) (Rabbit anti-mouse)	Cell Signaling	Cat# 4812S
Anti-β-Actin (mouse monoclonal)	Sigma	Cat#A5316
Anti-α-tubulin	Sigma	Cat# T5168
IRDye 800CW goat anti-Rabbit IgG	Li-Cor	Cat# 926-32211
IRDye 680RD goat anti-Mouse IgG	Li-Cor	Cat# 926-68070
FITC anti mouse CD3	Miltenyi Biotec	Cat# 130-119-758
PE anti mouse GzmA	BioLegend	Cat# 149703
PE mouse IgG2b	BioLegend	Cat# 400311
APC anti mouse CD8a	Miltenyi Biotec	Cat# 130-120-159
APC anti mouse CD4	Miltenyi Biotec	Cat# 130-116-526
APC-Vio770 anti mouse NK1.1	Miltenyi Biotec	Cat# 130-120-510
VioBlue anti mouse CD45	Miltenyi Biotec	Cat# 130-110-664
Chemicals, Peptides, and Recombinant Proteins		
Dextran Sulfate Sodium, Colitis grade 36.000–50.000	MP Biomedicals	Cat# 9011-18-1
Azoxymethane (AOM)	Sigma-Aldrich	Cat# A5486
FITC-Dextran	Sigma	Cat# FD4-100MG
Dulbecco's modified Eagle's medium (DMEM)	Sigma	Cat# 5796
Penicillin-Streptomycin (10.000 U/10 mg/ml)	Sigma	Cat# P4333
Fetal bovine serum (FBS)	Sigma	Cat# F2442
Trypsin-EDTA (0.25%), phenol red	Sigma	Cat# T4049-100ML
HBSS without Mg2+ and Ca^{2+}	Sigma	Cat# H6648-500ML
HEPES solution 1M	Sigma	Cat# H0887-20ML
2-mercaptoethanol	Sigma	Cat# M7522
Percoll	Sigma	Cat# P1644-100ML
Dithiothreiteol (DTT)	Sigma	Cat# 3383-12-3
Recombinant mouse GzmA	This paper	N/A
Recombinant mouse Serpinb6b	This paper	N/A
Cathepsin C	Sigma	Cat# 9032-68-2
Enbrel (Etanercept)	Gift from Dra. Ana María Ortiz García (La Princesa University Hospital, Madrid, Spain)	N/A
Bz-Pro-Phe-Arg-pNA.HCl	Bachem	Cat# 4012267
Critical Commercial Assays		
Mouse IL-1β ELISA Ready set Go! Kit	eBioscience	Cat# 88-7013-88
Mouse IL-6 ELISA Ready set Go! Kit	eBioscience	Cat# 88-7064-77
Mouse IL-10 ELISA Ready set Go! Kit	eBioscience	Cat# 88-7105-76
Mouse IL-17A ELISA Ready set Go! Kit	eBioscience	Cat# 88-7371-77
Mouse IFNγ ELISA Ready set Go! Kit	eBioscience	Cat# 88-73-84-21
Mouse TNFα ELISA Ready set Go! Kit Ready set Go! Kit	eBioscience	Cat# 88-7324-86
Mouse PGE_2 ELISA Kit	Arbor Assay	Cat# K051-H1
RNeasy Mini Kit	QIAGEN	Cat# 74104

(*Continued on next page*)

Continued

REAGENT or RESOURCE	SOURCE	IDENTIFIER
SYBR™ Green PCR Master Mix	Applied Biosystems	Cat# 4309155
SuperScript™ II Reverse Transcriptase	Invitrogen	Cat# 18064014
Deposited Data		
16S rDNA sequencing data	This paper	https://www.ncbi.nlm.nih.gov/sra/PRJNA634245
Experimental Models: Cell Lines		
Mouse: MC-38	Gift from Pedro Berraondo López (CIMA)	N/A
Experimental Models: Organisms/Strains		
Mouse: C57BL/6j Males (8-10 weeks)	Centro de Investigación Biomédica de Aragón; SCT Animal Facility	N/A
Mouse: GzmA^{KO} (on C57BL/6j background) Males (8-10 weeks)	Centro de Investigación Biomédica de Aragón; SCT Animal Facility	N/A
Oligonucleotides		
GZMA forward 5′-GGTGGAAAGGACTCCTGCAA-3′	ThermoFisher	N/A
GZMA reverse 5′-GCCTCGCAAAATACCATCACA-3′	ThermoFisher	N/A
COX-2 forward 5′-TGCCTCCCACTCCAGACTAGA-3′	ThermoFisher	N/A
COX-2 reverse 5′-CAGCTCAGTTGAACGCCTTTT-3′	ThermoFisher	N/A
HPRT forward 5′-CTGGTGAAAAGGACCTCTCGAA-3′	ThermoFisher	N/A
HPRT reverse 5′-CTGAAGTACTCATTATAGTCAAGGGCAT-3′	ThermoFisher	N/A
V3-4 Forward 5′-TCGTCGGCAGCGTCAGA TGTGTATAAGAGACAGCCTACGGGNGGC WGCAG	ThermoFisher	N/A
V3-V4 Reverse 5′-GTCTCGTGGGCTCGGAGATGTGTATAAGA GACAGGACTACHVGGGTATCTAATCC	ThermoFisher	N/A
Software and Algorithms		
GraphPad Prism 5	Graphpad Software	N/A
ImageJ	(Schneider et al., 2012)	https://imagej.nih.gov/ij
Weasel 3.3.2	Weasel Software	N/A

RESOURCE AVAILABILITY

Lead Contact

Further information and requests for resources and reagents should be directed to and will be fulfilled by the Lead Contact, Julián Pardo (pardojim@unizar.es)

Materials Availability

Recombinant mouse Granzyme A generated in this study is available from the Lead Contact without restriction.

Data and Code Availability

The 16S rDNA sequencing data generated during this study is available at https://www.ncbi.nlm.nih.gov/sra/PRJNA634245.

EXPERIMENTAL MODEL AND SUBJECT DETAILS

Human samples

Gene expression data from a set of 98 tumor tissues from CRC patients was used (Colonomics project: https://www.colonomics.org, NCBI BioProject PRJNA188519). Briefly, RNA extracted from each sample was hybridized in Affymetrix chips Human Genome U219 and analyzed under standard protocol (Sanz-Pamplona et al., 2014). Both raw and normalized data are available in the Gene Expression Omnibus (GEO) database through accession number GSE44076. All patients were stage II, MSS, treated with radical surgery and did not received adjuvant chemotherapy. They were recruited at the Bellvitge University Hospital (Spain) between 1998 and

2002, provided written informed consent and the hospital Ethics Committee approved the protocol with reference PR074/11. Patients' characteristics are summarized in Table S1.

Mice

Inbred C57BL/6 (Wt), and mouse strains deficient (knockout/KO) for granzyme A ($GzmA^{KO}$/$GzmA^{-/-}$) on the B6 background were bred and maintained at the CIBA (Centro de Investigación Biomédica de Aragón; SCT Animal Facility). Their genotypes were periodically analyzed as described (Pardo et al., 2008). Animal experimentation was approved by the Ethics Committee for Animal Experimentation from University of Zaragoza (protocol number PI17/15). Male 8-10-week-old mice were used for all experiments. To control that the differences between Wt and $GzmA^{KO}$ animals were not affected by minor differences in genetical backgrounds and/or other factors control littermates were employed in some experiments.

Cells lines and primary cell cultures

Primary M1 macrophages were differentiated from bone marrow of C57BL/6 mice. Cells were aseptically collected from bone marrow and resuspended in RPMI 1640 medium containing 10 % of FCS serum, 100 U/ml of penicillin/streptomycin, 50 mM of 2-ME, and 10 % of supernatant of X63Ag8653 cell cultures as source of GM-CSF (74) (GM-CSF medium). Cells were cultured on 100 mm Petri dishes, 1×10^6 cells/ml in 10 mL GM-CSF culture medium and allowed to differentiate for 7 days at 37°C and 5 % CO2. On days 3 and 5, the supernatant was removed, adherent cells were washed twice with PBS and 10 mL of fresh GM-CSF medium was added. On day 7, cells showed differentiated morphology and expressed the macrophage markers CD11b+ F4/80+.

MC-38 cells, a cell line derived from a colon adenocarcinoma (kindly given to our group by Dr. Pedro Berraondo López, researcher at Center for Applied Medical Research (CIMA), University of Navarre), were cultured in DMEM medium (supplemented with 2 mM L-glutamine, 100 U/ml penicillin, 100 U/ml streptomycin, and 10 % FBS) at 37°C, in a 5 % CO_2 atmosphere.

METHOD DETAILS

Transcriptomics analyses in human samples

Transcriptomic data from human CRC tissues were used to explore genes whose expression was associated with GZMA and GZMB expression. Spearman's correlation was calculated to generate a ranked gene list sorted by their level of co-expression with both genes. Then, the Gene Set Enrichment analysis (GSEA) algorithm (Subramanian et al., 2005) was used on these pre-ranked lists to identify enrichment in specific cellular functions and pathways. Specifically, the Hallmarks gene sets were interrogated.

The Gene Set Variation Analysis from GSVA R package was used to calculate an inflammatory score using the *Positive Regulation of Inflammatory Response* gene set from Gene Ontology (GO). This function performs a non-parametric, unsupervised analysis for estimating variation of the given gene sets through the samples in the expression matrix, returning an enrichment score for each sample. Also, a heat-map was plotted with all genes included in the gene set for visualization purposes (Figure S1A).

Spearman's correlation was calculated to assess if there is a relationship between the inflammatory score and the GZMA/GZMB expression. The same analysis was done stratifying samples into CMS subtyping. Linear regression models were also adjusted to calculate R-squared and p values in each case.

To validate these results, an extended gene expression dataset was downloaded from GEO repository (GSE39582). This comprises 566 CRC human samples with distinct clinicopathological characteristics, which underwent surgery between 1987 and 2007. It includes patients from 0 to IV stage, both MSI and MSS and receiving different treatments (Marisa et al., 2013). Finally, tumors from both datasets were classify into the four consensus molecular subtypes CMS1 to CMS4 using the CMS classifier R package (Guinney et al., 2015).

Induction of Colitis and Colitis-associated Colorectal Cancer

Induction of acute or chronic colitis and colitis associated colorectal cancer (CAC) was performed as previously described employing a combination of DSS and AOM (Neufert et al., 2007; Wirtz et al., 2007). In brief, acute colitis was induced through administration of 2.5 % DSS (MW 36,000–50,000 from MP) in drinking water for five days. Chronic colitis was induced by 3 cycles of 2.5 % DSS in drinking water for five days followed by normal drinking water for 2 weeks. Colorectal cancer was induced by intraperitoneal injection of a single dose of the mutagenic agent AOM (10 mg/kg, Sigma Aldrich) on day 1 followed by 3 cycles of 2.5 % DSS in drinking water for five days and normal drinking water for 2 weeks.

Clinical score

Mice were weighed and observed daily. The scoring system assigns severity scores to five different parameters: weight loss, stool consistency, fecal blood, mouse behavior and dehydration. The final clinical score results from the addition of individual scoring, with a maximum of 24 points per mouse. The scoring system assigns severity values to five parameters: Weight changes (< 1 % = 0; 1-5 % = 1; 5-10 % = 2; 10-20 % = 3; > 20 % = 4), Stool Consistency (Normal = 0; soft feces = 1; diarrhea = 4), Visible Bleeding (No visible = 0; visible bleeding = 4), Mouse Behavior (Normal = 0; slight changes = 1 abnormal = 4; immobility = 8) and Dehydration (Normal = 0; dehydration = 4).

Macroscopic damage score

Animals were sacrificed, the colon was measured and weighed and the visible colonic damage was scored. The scoring system assigns severity values to six parameters: Diarrhea (normal = 0; soft = 1; liquid = 4), Bleeding (No = 0; Yes = 4), Erythema (No = 0; Mild and/or localized = 1; intense and/or generalized = 2), Edema (No = 0; Mild and/or localized = 1; intense and/or generalized = 2), Stenosis (No = 0; 1 Stenosis = 1; 2 Stenosis = 2; > 2 Stenosis = 3) and Adhesions (No adhesions = 0; Difficult dissection = 1; Visible adhesions = 2; ¨Wrapped¨ intestine = 3). Similarly to clinical evaluation, the final macroscopic damage score was obtained by the addition of individual scoring. The incidence of tumors as well as number and tumor diameter when present were also quantified.

Histological Scoring of Inflammation and tumor grading

Colon tissues were removed from mice, fixed with 4 % paraformaldehyde, and embedded in paraffin. Sections from these samples were stained with hematoxylin and eosin (H&E). Scoring of inflammation was performed according to previous works (Izcue et al., 2008). Briefly, each sample was graded semiquantitatively from 0 to 3 for the four following criteria: degree of epithelial hyperplasia and goblet cell depletion, leukocyte infiltration in the lamina propria, area of tissue affected, and presence of markers of severe inflammation (such as crypt abscesses, submucosal inflammation, and ulcers). Scores for each criterion were added to give a final quantification for intestinal inflammation ranging from 0 to 12. The total colonic score was calculated as the average of the individual values from the colonic sections. Blinded samples were analyzed by an expert pathologist.

Low-grade dysplasia, high-grade dysplasia, and adenocarcinoma were blindly scored using criteria for grading dysplasia in human IBD (Boulard et al., 2012), as well as the TNM classification of colorectal tumors (Sobin and Compton, 2010). Criteria for dysplasia in human IBD: low grade dysplasia, requires intact to mild alteration of gland architecture and nuclear alterations that extend to mucosal surface without appreciable loss of nuclear polarity; high grade dysplasia, involves intact to severe alterations of gland architecture with clear evidence of a loss of nuclear polarity. TNM classification of colorectal tumors grades the level of tumor invasiveness, from carcinoma *in situ* to invasion of submucosa. Photomicrographs of H&E and immunostained colon sections were taken with an Axioplan 2 microscope equipped with an AxioCamHRc camera and the Axiovision 4.6 image analysis software package (Zeiss).

Immunohistochemistry

Immunohistochemistry was carried out using the following antibodies: β-Catenin (1/300), anti-Ki-67 (1/200) and anti-Vimentin (1/100) (all BD Biosciences), anti-pSTAT3 (Cell Signaling; dilution 1/200), and anti-SNAIL (tissue culture supernatant).

Immunohistochemical (IHC) analyses were performed using 3 μm sections of formaldehyde-fixed, paraffin-embedded tissue blocks. Antigen retrieval was done by boiling the slides in 10 mM sodium citrate pH = 6,6 for 10 min (E-Cadherin, Ki-67 and Vimentin); sub-boiling in 10 mM Tris base, 1 mM EDTA pH = 9 for 15 minutes (β-Catenin, SNAIL1) or sub-boiling for 15 minutes in 1 mM EDTA pH = 8 (pSTAT3). Slides were blocked with filtered 5 % non-fat milk dissolved in PBS (in TBS plus 0.1 % Tween-20 in the case of pSTAT3 and SNAIL).

In the case of SNAIL, after endogenous peroxidase-blocking cells were permeabilized with TBS containing 1% Triton X-100 and 1 % Tween-20 for 30 minutes at room temperature and washed twice with TBS plus 0.1 % Tween-20. For blocking, cells were incubated 2 hours at room temperature with NGBS (10 % Normal goat serum, 1 % BSA, 0.1 % Cold fish gelatin, 0.1 % Triton X-100, 0.05 % Tween-20, 0.05 % sodium azide) (Francí et al., 2006).

Primary antibodies were diluted in PBS containing 1 % BSA (except in the case of SNAIL for which 1% of NGBS was added to the tissue culture supernatant of the hybridoma) and were incubated for 90 min at 37°C or o/n at 4°C. As secondary antibody, the corresponding HRP-labeled secondary antibody or anti-mouse or rabbit PowerVision™ (Leica Biosystems) were used. The HRP colorimetric substrate TMB (Vector) was used for visualization. Sections were counterstained with hematoxylin, dehydrated, and mounted.

Positive cells were enumerated on 5 randomly chosen visual fields for each tissue sample with the aid of ImageJ software. For Ki-67, the percentage of positively stained nuclei was determinates using the ImmunoRatio image analysis software, as an open source of ImageJ plugin or as a freely accessed online program for image analysis from immunohistochemistry (Tuominen et al., 2010). Immunohistochemistry stained slides were visualized and scanned on a ZEISS Axio Scan.Z1 at 20 X magnification.

Quantitative real-time RT-PCR

RNA extractions were carried out with the RNeasy mini kit (QIAGEN, Hilden, Germany) following the manufacturer's instructions, as previously described (Matheus et al., 2009). Total RNA was extracted from distal and proximal colonic tissue. cDNA was subsequently generated with SuperScript II reverse transcriptase (Invitrogen Life Technologies).

Quantitative real-time PCR was performed with StepOne Plus PCR system (Invitrogen Life Technologies) in combination with specific primers for *GZMA* and COX-2 on the iQiCycler (Bio-Rad, Hercules, CA) according to a standard protocol (40 cycles, annealing temperature 60°C). Relative levels of mRNA expression were normalized to HPRT mRNA levels using a comparative method ($2^{-\Delta\Delta Ct}$). Each sample was run in triplicate, and the mean Ct was determined. Relative *GZMA* expression under each experimental condition (control or treatment) was expressed as $\Delta Ct = Ct_{GZMA} - Ct_{calibrator}$, being HPRT housekeeping gene expression used as calibrator. Then relative *GZMA* mRNA expression was calculated as $\Delta\Delta Ct = \Delta Ct_{control} - \Delta Ct_{treatment}$. Finally, the relative gene expression levels were expressed as fold difference ($2^{-\Delta\Delta Ct}$). All primer sequences are listed in the Key Resources Table.

Measurement of cytokine, PGE2 and GzmA levels in cultures of colonic tissue explants

Intestine pieces were cut out, weighed (30 mg) and maintained in culture medium (2 ml, DMEM containing 10 % FBS, 10 mM glutamine, 10 mM HEPES and 100 U/ml of penicillin/streptomycin) at 37°C in an atmosphere of 5 % CO_2. After 24h, supernatants were collected, centrifuged at 500 xg for 10 min and aliquots were stored at −80°C for ELISA analysis (Han et al., 2010).

Levels of IL-1β, TNF-α, IFN-γ, IL-6, IL-10 and IL-17 in supernatants were quantified with the respective Ready-SET-Go! ELISA Sets from eBioscience. Prostaglandin E_2 (PGE_2) was analyzed with an ELISA kit from Arbor Assay following manufacturer's instructions.

A conventional indirect sandwich ELISA to detect mouse GzmA has been previously described (Santiago et al., 2017).

Isolation of colon IEL cells and GzmA intracellular expression analysis

IEL cells from colon intestine were obtained from DSS/AOM treated mice and from untreated mice. In brief, a colon free of the lumen were cut in small pieces and transferred to a 50 mL conical tube with 20 mL of pre-digesting solution (HBSS buffer containing 10 % of FBS, 5 mM EDTA and 1 mM DTT). The tissue was incubated at 37°C for 25 min with gentle shaking. After vortex sample vigorously for 10 s, intestinal fragments were removed by passing through a 100 μm cell strainer. Residual tissues were incubated again in the same manner. Cell suspensions were pooled and washed with RPMI medium containing 10 % of FBS. To isolate a lymphoid cell fraction, the cells were centrifuged in a 40%/80% Percoll gradient (Sigma Aldrich, Spain) at 700 xg for 20 min at room temperature. Cells from the 40%/80% Percoll interface were collected, washed, and counted.

Colon IEL cells were stained with a combination of FITC conjugated anti CD3, APC conjugated anti CD8a, APC-Vio770 conjugated anti NK1.1 and VioBlue conjugated anti CD45 antibodies from MiltenyiBiotec. Subsequently, cells were fixed with paraformaldehyde (PFA) 1 %, then permeabilized with saponin 1 % in PBS 5 % FBS and incubated with PE conjugated anti GzmA (eBioscience) or with the isotype (IgG-PE) (eBioscience). Finally, intracellular expression of GzmA was analyzed by FACS.

GzmA activity assay

GzmA protease activity on Bz-Pro-Phe-Arg-pNA-HCl (BACHEM) substrate was tested spectrophotometrically using Multi-Mode Microplate Reader (Synergy HT, BioTek) as previously described (Martin et al., 2005). Briefly, 50 μL of supernatant from cultures of colonic tissue explants were dissolved in 50 μL of 100 mM Tris/HCl; pH 8.5 (GzmA activity buffer). A soluble protein extract from the $CD8^+$ T cell line 1.3E6SN (cytotoxic T-lymphocyte line; CTLL), or from the mouse tumor cell line EL4.F15 used as positive and negative controls, respectively. Then, Bz-Pro-Phe-Arg-pNA-HCl substrate (50 μl/well, end concentration 150 μM in GzmA activity buffer) was added and incubated at 37°C. Optical density (OD) at 405/490 nm was measured after 0′; 60′; 120′ and overnight. All measurements were implemented by duplicate or triplicate. The specific activity of GzmA was represented as moles of substrate converted by the enzyme per minute and per milligram of protein in a sample.

Expression and purification of recombinant GzmA and Serpinb6b

Recombinant mouse GzmA was produced in *E.coli* B834 (DE3) and purified by cation-exchange chromatography as previously described for GzmB (Pardo et al., 2007). GzmA was produced as an inactive pro-enzyme (proGzmA), which was then activated by cathepsin C to generate the active enzyme. Enzymatic activity of all preparations was analyzed as described above.

Recombinant mouse Serpinb6b was produced as His-tagged protein in *P. Pastoris* (SMD1163) and purified by immobilized metal (Nickel) affinity chromatography as previously described (Kaiserman et al., 2014).

Analysis of IL-6 expression induced by extracellular GzmA in M1 macrophages

Recombinant mouse GzmA and Serpinb6b were produced in *E.coli* and *P. Pastoris* as previously described (Kaiserman et al., 2014; Pardo et al., 2007). Pro-inflammatory M1 macrophages were generated from bone marrow using GM-CSF as growth factor.

Macrophages were stimulated with active GzmA (300 nM) or GzmA inactivated with the specific inhibitor serpinb6b (2.4 μM) and *E. coli* LPS 100 ng/ml. NF-kB, caspase-1 and COX-2 pathways were blocked with specific inhibitors of NF-kB (Celastrol), caspase-1 (VX765) or COX-2 (Celecoxib) during 1h before the addition of GzmA. IL-6 was measured by ELISA in cell supernatants after 24h.

In vivo treatments

Extracellular GzmA was inhibited using a specific mouse GzmA inhibitor, serpinb6b. CRC was induced as indicated above. On day 35 a group of mice were treated with five doses of serpinb6b 20 μg iv every other day. A group of mice were treated with serpinb6b previously inactivated with trypsin as a control. Mice were sacrificed at day 49; macroscopic score, incidence, number, and size of tumors were analyzed. A portion of colon was cultured as indicated above to determine the level of inflammatory cytokines.

In vivo TNFα was inhibited using a human TNF specific antagonist, Enbrel (etanercept). CRC was induced as previously described. On day 56 mice were treated with five daily doses of Enbrel (5 mg/kg ip). On necropsy, incidence, number, and size of tumors were analyzed. In addition, a colonic tissue samples (30 mg) were cultured during 24 h, supernatant was collected and the levels of TNF-α was quantified by ELISA.

In order to analyze the steady-state intestinal permeability *in vivo*, Wt and $GzmA^{KO}$ healthy mice were treated with FITC-dextran dissolved in PBS (100 mg/ml). Each mouse received 44 mg/100 g of body weight by oral gavage with a needle attached to a 1 mL syringe. After 4 h, mice were sacrificed and blood was collected, then serum was separated and stored at 4°C in the dark. 100 μL of

diluted serum (1:1 in PBS) were added to a 96-well microplate in duplicate. The concentration of FITC in serum was quantified by spectrophoto fluorometry with an excitation of 485 nm following manufacturer's instructions.

Western blot

MC-38 cells were seeded (1 × 10^6 cel/wells) in DMEM medium (supplemented with 2 mM L-glutamine, 100 U/ml penicillin, 100 U/ml streptomycin, and 10 % FBS). After 4 h, cells were changed into DMEM medium without SFB, and cultured for 16 h at 37°C. Subsequently, the medium was removed and supernatant from recombinant mouse GzmA-stimulated macrophage (300 nM) or supernatant from LPS-stimulated macrophage (100 ng/ml) were added. Supernatant from unstimulated macrophage were use as control. As a positive control, 50 ng/ml of mouse IL-6 (Miltenyi) was added. The cells were lysed 15 minutes after the addition of the stimuli. The concentration of total proteins was determined using Quick StartTM Bradford Protein Assay (BioRad). Finally, a western blot was performed using the corresponding antibodies to visualize and quantify the expression of pSTAT3.

Gut microbiota composition

Faces from both Wt and $GzmA^{KO}$ were collected after gently perianal stimulation. After a complete mixing of the sample by vortex, total DNA was obtained using the QIAamp DNA Mini Kit (QIAGEN, Germany), adequate controls of quality and concentration, DNA samples were sent to the FISABIO institution (http://fisabio.san.gva.es) for massive sequencing of 16S rDNA amplicons of the V3 and V4 regions were amplified with the appropriate primers (Quast et al., 2013). The primers sequences are listed in the Key Resources Table.

Taxonomic affiliations were assigned using SILVA_release_119 database (Quast et al., 2013). The statistical analysis was performed using R statistical software and open source libraries. The quantitative data of the reads were homogenized using their relative percentage from the total reads of each sample to facilitate the comparison between samples. Finally, Galaxy Huttenhower Platform (http://huttenhower.sph.harvard.edu/galaxy) was used in order to calculate LefSe (LDA Effect Size) algorithm and to obtain cladograms in which microbial taxa that explain significant differences among groups of samples were represented.

QUANTIFICATION AND STATISTICAL ANALYSIS

Statistical analysis was performed using GraphPad Prism 5 software using the test indicated in the corresponding figure legends. Data are presented as mean ± SEM. The difference between means of unpaired samples was performed using the two-way ANOVA or the one-way ANOVA with Bonferroni's post-test or using un-paired t test. Survival curves were compared using both the log rank test and the Gehan-Wilcoxon test. The tumor incidence was analyzed using a Fisher's exact test. The results are given as the confidence interval (p), and are considered significant when $p < 0.05$. Biological replicates are considered as the number of individual mice.

In human tumor samples Spearman's correlation was calculated to assess the relationship between the inflammatory score and the *GZMA* / *GZMB* expression. The same analysis was done stratifying samples into CMS subtyping. Linear regression models were also adjusted to calculate R-squared and p values in each case